https://doi.org/10.5194/egusphere-2022-1005
Preprint. Discussion started: 18 October 2022

A practical method for assigning uncertainty and improving the accuracy of alpha-ejection corrections and eU concentrations in apatite (U-Th)/He chronology

Spencer D. Zeigler[1], James R. Metcalf[1], Rebecca M. Flowers[1]

[1]Department of Geological Sciences, University of Colorado Boulder, Boulder, CO, 80309, USA

Correspondence to: Spencer D. Zeigler (spencer.zeigler@colorado.edu)

Abstract. Apatite (U-Th)/He (AHe) dating generally assumes that grains can be accurately and precisely modeled as geometrically perfect hexagonal prisms or ellipsoids in order to compute the apatite volume (V), alpha-ejection corrections (F_T), equivalent spherical radius (R_{FT}), effective uranium concentration (eU), and corrected (U-Th)/He date. It is well-known that this assumption is not true. In this work, we present a set of corrections and uncertainties for V, F_T, and R_{FT} aimed at 1) "undoing" the systematic deviation from the idealized geometry and 2) quantifying the contribution of geometric uncertainty to the total uncertainty budget on eU and AHe dates. These corrections and uncertainties can be easily integrated into existing laboratory workflows at no added cost, can be routinely applied to all dated apatite, and can even be retroactively applied to published data. To quantify the degree to which real apatite deviate from geometric models, we selected 267 grains that span the full spectrum of commonly analyzed morphologies, measured their dimensions using standard 2D-microscopy methods, and then acquired 3D scans of the same grains using high-resolution computed-tomography. We then compared the V, F_T, and R_{FT} calculated from 2D-microscopy measurements with those calculated from the 'real' 3D measurements. We find that apatite V, F_T, and R_{FT} values are all consistently overestimated by the 2D microscopy method, requiring correction factors of 0.74-0.83 (or 17-26%), 0.91-0.99 (or 1-9%), and 0.85-0.93 (or 7-15%), respectively. The 1s uncertainties on V, F_T, and R_{FT} are 20-23%, 1-6%, and 6-10%, respectively. The primary control on the magnitude of the corrections and uncertainties is grain geometry, with grain size exerting additional control on F_T uncertainty. Application of these corrections and uncertainties to a real dataset yields 1s analytical and geometric uncertainties of 15-16% on eU and 3-7% on the corrected date. These geometric corrections and uncertainties are substantial and should not be ignored when reporting, plotting, and interpreting (U-Th)/He datasets. The Geometric Correction Method presented here provides a simple and practical tool for deriving more accurate F_T and eU values, and for incorporating this oft neglected geometric uncertainty into AHe dates.

https://doi.org/10.5194/egusphere-2022-1005
Preprint. Discussion started: 18 October 2022

1 Introduction

(U-Th)/He dating is a widely-applied thermochronologic technique used to decipher low-temperature thermal histories. In addition to analysis of parent and daughter isotopes, the conventional whole crystal (U-Th)/He method typically includes microscopy measurements of the analyzed grain. These measurements are combined with an assumed idealized grain morphology to estimate the grain volume (V) and surface area, which in turn are used to calculate three important parameters: the alpha-ejection correction (F_T value), the effective uranium concentration (eU), and the equivalent spherical radius. F_T values are required for accurate dates on crystals that are not fragments, because ^{4}He atoms travel ~20 µm during α-decay and a correction is required to account for He lost by this effect (e.g., Farley et al., 1996; Ketcham et al., 2011). eU is important for accurate (U-Th)/He data interpretation because radiation damage scales with eU, which affects He retentivity (e.g., Shuster et al., 2006; Flowers et al., 2007). The equivalent spherical radius is used to approximate the diffusion domain of whole crystals, and is a standard parameter needed for diffusion modeling (here we use a sphere with an equivalent F_T correction as the analyzed grain and refer to this parameter as R_{FT}).

It is well-recognized that there is both uncertainty and potentially systematic error associated with the microscopy approach to calculating geometric data and the parameters derived from them (Ehlers and Farley, 2003; Herman et al., 2007; Evans et al., 2008; Glotzbach et al., 2019; Cooperdock et al., 2019; Flowers et al., 2022a). Throughout this paper we use "uncertainty" to refer to the reproducibility of measurements, and "error" to refer to a systematic deviation between a measured value and the true value (JCGM, 2012). Conceptually, Figure 1 shows how the commonly assigned hexagonal and ellipsoid grain geometries for apatite can lead to deviations from the true volumes and surface areas of real grains. Early work suggested that these deviations could cause as much as ± 25% uncertainty on the F_T values for hexagonal, prismatic apatite grains of 50 µm width, decreasing to <2% for grains with cross-sections of >125 µm (Ehlers and Farley, 2003). Geometric uncertainties and systematic error have also been explored using x-ray micro- or nano-computed tomography (CT), a non-destructive method that creates 3D models of scanned objects (Herman et al., 2007; Evans et al., 2008; Glotzbach et al., 2019; Cooperdock et al., 2019). These studies presented new, more comprehensive techniques for 2D grain measurements (the 3D-He method of Glotzbach et al., 2019) and proposed a method to routinely acquire CT data for all dated apatite grains (Cooperdock et al., 2019).

Despite this past work, the uncertainties on the grain's geometric information are not typically propagated into the uncertainties of the derived parameters (e.g., eU concentration, corrected (U-Th)/He date). Nor are data systematically corrected for potential error associated with grain measurements. This is largely because uncertainty and error in the geometric parameters depend in large part on how much the real grain geometry deviates from that assumed, which may vary from grain to grain, depending on grain morphology, as well as possibly on grain size and other parameters. Moreover, although both the 3D-He method (Glotzbach et al., 2019) and the routine CT analysis approach (Cooperdock et al., 2019) would improve the accuracy and precision of geometric parameters, both add more time to the (U-Th)/He dating process, and in the case of the latter, requires regular access to CT instrumentation.

https://doi.org/10.5194/egusphere-2022-1005
Preprint. Discussion started: 18 October 2022

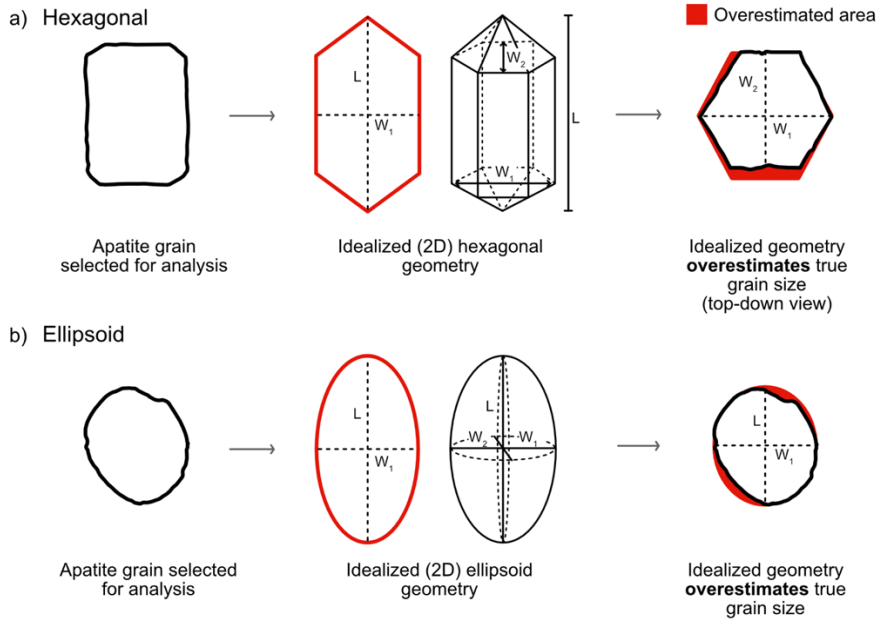

Figure 1. Examples of realistic (a) hexagonal and (b) ellipsoid apatite grains (left column) versus the idealized geometry that is used to calculate V, F_T, and R_{FT} (middle column). In the right column, the 'real' grain is overlaid onto the idealized geometry in red. The shaded area in red is the portion of the grain that is erroneously included by the use of an idealized geometry. For both hexagonal and ellipsoid shapes, the idealized geometry overestimates the real apatite volumes.

However, rigorous quantification of uncertainties and corrections for systematic error are required to represent and interpret (U-Th)/He data accurately. For example, appropriate uncertainties on single-grain dates are important for deciding if data are normally distributed and thus reasonable to represent and model as a mean sample date, or if the data are "overdispersed" (e.g., Flowers et al., 2022b). Similarly, appropriate uncertainties on other parameters such as eU are needed to properly decipher AHe date vs. eU patterns.

To address this problem, we present a time-efficient and straightforward "geometric correction" method to routinely correct for systematic error and to assign uncertainties to F_T, eU, and R_{FT} values for the full spectrum of regularly analyzed apatite grain sizes and morphologies. This approach requires no additional work or cost beyond what is already done as part of most existing (U-Th)/He dating workflows. Nor does it necessitate additional microscopy measurements or routine CT analysis of grains, so it is easily adoptable by any lab or data user. Additionally, this method can be applied retroactively to previously collected data, even after the grains themselves have been dissolved and are no longer available for additional work. We first developed a simple classification system for apatite grains of varying morphology and surface roughness. For 237 apatite crystals characterized by a wide range of morphology, size, age, and lithologic source, we then compared V, F_T, and R_{FT} estimates calculated from 2D microscopy measurements with those determined by CT scans of the same grains at 0.64 μm resolution. We use these data to derive corrections for systematic error and to determine

https://doi.org/10.5194/egusphere-2022-1005
Preprint. Discussion started: 18 October 2022

uncertainty values that can be applied to 2D V, F_T, and R_{FT} values depending on the geometry and size of the analyzed apatite. These outcomes allow analysts to 1) correct geometric parameter values for systematic error, 2) propagate the F_T uncertainty into the reported uncertainty on corrected (U-Th)/He dates, 3) propagate the V uncertainty into the reported uncertainty on eU values, and 4) report R_{FT} value uncertainties that have potential to be included in thermal history modeling. We conclude by illustrating this approach with real (U-Th)/He data and discuss the implications for the accuracy and precision of (U-Th)/He datasets more broadly.

2 Background

2.1 F_T, eU, and Rs values in (U-Th)/He thermochronology

An important consideration for the (U-Th)/He system is alpha-ejection. During radioactive decay of the parent isotopes (^{238}U, ^{235}U, ^{232}Th, ^{147}Sm), ^{4}He atoms are ejected from the parent atom (e.g., Farley et al., 1996). Alpha particles, or helium atoms, will travel a certain distance related to the density of the mineral through which they travel and the ejection energy from the parent atom. For apatite, the average stopping distances for ^{238}U, ^{235}U, and ^{232}Th, are 18.81 µm, 21.80 µm, and 22.25 µm, respectively, and for ^{147}Sm it is 5.93 µm (e.g., Ketcham et al., 2011). If the parent atom is positioned within the ejection range of the grain edge, then the He atom has a non-zero chance of being ejected from the crystal entirely. The probability of retention increases with increasing distance of the parent from the grain edge. Overall, the smaller the grain, the higher the surface area to volume ratio of the grain, and the greater percentage of He that is lost via the ejection process.

To obtain an intuitively more meaningful date, (U-Th)/He dates on crystals that retain their original grain edge are typically corrected for the He lost by alpha ejection to obtain a "corrected (U-Th)/He date". This alpha-ejection correction (or F_T value) is the fraction of He that is retained in the crystal, such that an F_T value of 0.70 means that an estimated 30% of He was lost from the crystal by ejection. F_T is typically calculated based on the stopping distances of He in each mineral for each parent isotope, the proportion of the parent isotopes, the crystal dimensions, and an assumed idealized crystal geometry that enables one to use the crystal measurements to estimate the surface area and volume of the crystal (Farley et al., 1996). F_T corrections typically assume a uniform distribution of parent isotopes; parent isotope zonation in crystals can introduce additional uncertainty into the F_T correction (Farley et al., 1996; Meesters and Dunai, 2002; Hourigan et al., 2005). Additional uncertainty can also arise for broken or abraded crystals, where the magnitude of the appropriate correction can be unclear (Brown et al., 2013).

The effective U concentration (eU) is important for (U-Th)/He thermochronology because it can be used as a proxy for radiation damage, which can have a large effect on the mineral He retentivity (e.g., Shuster et al., 2006; Flowers et al., 2007). Accurate eU values depend on accurate grain volumes, because volumes are used to calculate grain masses, which in turn are used to compute parent isotope concentrations and eU (e.g., Flowers et al., 2022a).

https://doi.org/10.5194/egusphere-2022-1005
Preprint. Discussion started: 18 October 2022

The equivalent spherical radius is relevant for (U-Th)/He thermochronology because mineral diffusion depends on grain size. Grain size is therefore included in the diffusion modeling used to decipher thermal histories from (U-Th)/He data. The equivalent spherical radius parameter can be reported either as a sphere with the same surface area to volume ratio as the analyzed grain, or as a sphere with the same F_T value as the analyzed grain (R_{FT}, Ketcham et al., 2011; Cooperdock et al., 2019). Use of R_{FT} is preferred, because during thermal history modeling this value yields outcomes more similar to those using the real 3D grain geometries (Ketcham et al., 2011; Flowers et al., 2022a).

2.2 Use of CT for F_T, eU, and R_{FT} value determinations

Computed tomography (CT) is a high-resolution (sub-micrometer), non-destructive, 3D imaging technique based on the attenuation of x-rays through a sample. 2D cross sections ('slices') of the sample are created as x-rays pass through the sample and are then processed into 3D models. These models can be analyzed with software like Dragonfly and Blob3D to extract high quality 3D dimensional and geometric data like volume and surface area (Ketcham, 2005; Dragonfly, 2020).

CT has been applied to improve the accuracy of geometric parameters in (U-Th)/He chronology in four studies (Herman et al., 2007; Evans et al., 2008; Glotzbach et al., 2019; Cooperdock et al., 2019). Initial work used CT data at a 6.3 µm resolution to derive F_T values for 11 irregularly shaped detrital apatite grains (Herman et al., 2007). This study then dated the crystals by (U-Th)/He and combined the 3D CT models of the dated grains with an inversion algorithm to constrain a range of thermal histories.

The subsequent studies have directly compared geometric parameters determined from 2D microscopy data with 3D CT measurements of the same grains. Evans et al. (2008) scanned 9 euhedral to subhedral, detrital and volcanic apatite and zircon grains at a 3.8 µm resolution, used the CT data to erode the outer 20µm of the scanned grain in 3D, and recalculated the "effective F_T" (Evans et al., 2008). Glotzbach et al. (2019) developed an improved microscopy method, called the 3D-He approach, to estimate F_T values using dimensions measured from a suite of photomicrographs to simulate a 3D grain model. They acquired CT data at 1.2 µm resolution for 24 apatite grains, including rounded, pitted, broken, anhedral, subhedral, and euhedral crystals. Cooperdock et al. (2019) presented a method for regular CT characterization of grains at 4-5 µm resolution and acquired CT data for a suite of 109 high quality euhedral apatite crystals from two plutonic samples. These three studies found that the 2D data variably over- or underestimated the 3D data for V, F_T, and R_{FT}, and estimated a range of scatter for the different parameters. These previous results are discussed in greater detail in Sect. 6.2 where we compare the outcomes of our study with this past work.

https://doi.org/10.5194/egusphere-2022-1005
Preprint. Discussion started: 18 October 2022

3 Selecting and Characterizing a Representative Apatite Suite

3.1 Strategy

We designed our study to ensure that we captured the range of representative apatite crystals commonly dated by the (U-Th)/He method. Our goal was to include the full spectrum of grain qualities in realistic proportions so that the study outcomes are relevant for the complete range of routinely analyzed grains. As described in more detail below, grain selection focused primarily on including crystals from samples encompassing a spectrum of lithology and age (Sect. 3.2), with a range of sizes (Sect. 3.3), and with variable morphology (Sect. 3.4). We ultimately selected 400 apatite grains for analysis, from which we obtained high-quality CT data for 267 crystals.

3.2 Selecting a Representative Sample Suite

Apatite grains were selected from eight samples that include six igneous and metamorphic rocks and two clastic sedimentary rocks with ages from Oligocene to Archean (Table 1). All samples were separated using standard crushing, density, and magnetic separation techniques. Most samples were dated previously by apatite (U-Th)/He (AHe) in the CU TRaIL (Thermochronology Research and Instrumentation Lab). The Oligocene Fish Canyon Tuff (sample FCT) from the San Juan Mountains in Colorado, USA is commonly used as a (U-Th)/He reference standard, with AHe dates younger than emplacement (e.g., Gleadow et al., 2015). The Eocene granitic Ipapah pluton is from the Deep Creek Range (sample DCA) of east-central Nevada, USA and yields Miocene AHe dates (unpublished data). The Cretaceous Whitehorn granodiorite (sample BF16-1) is from the Arkansas Hills in Colorado, USA and yields Eocene AHe dates (Abbott et al., 2022). The Cambrian McClure Mountain syenite (sample MM1) from the Wet Mountains of south-central Colorado yields Mesozoic AHe dates (Weisberg et al., 2018). A Proterozoic granitic dike from the Baileyville drill core (sample Bail933) in northeastern Kansas, USA yields Paleozoic AHe results (Flowers and Kelley, 2011). An Archean gneiss from the Superior craton in Canada (sample C50) yields Cambrian AHe dates (TraIL unpublished data). The two detrital samples (samples 16MFS-05 and 15MFS-07) have Cretaceous depositional ages, are from the Kaikoura Range on the South Island of New Zealand, and yield late Miocene to Pliocene AHe dates (Collett et al., 2019; Harbert et al, in review).

3.3 Selecting a Representative Crystal Size Distribution

The size distribution of grains analyzed in this study is based on the size distribution of grains routinely analyzed for (U-Th)/He dates. We first plotted the maximum width of apatite grains (N = 1061; Fig. 2) analyzed in the CU TRaIL over a two-year period. The grains in this dataset were from a variety of sources and were selected and measured by TRaIL staff, TRaIL students, and visitors. Our analysis focused on crystal width because the smallest dimension (i.e., the width) is the chief control on alpha-ejection due to the long stopping distances of alpha particles.

https://doi.org/10.5194/egusphere-2022-1005
Preprint. Discussion started: 18 October 2022

Table 1. Apatite sample information.

Sample Name	Sample Age	Lithology	Locality	Longitude (°W)	Latitude (°N)	GEM Categories	N[a]	Additional Geochronologic and Thermochronologic Data
Fish Canyon Tuff	Oligocene	Dacite	San Juan Mountains, Colorado, USA	-106.93	37.76	A1, A2, B1	31	Zircon U-Pb 28.172 ± 0.028 Ma (2s) (Schmitz and Bowring, 2001); AHe 20.8 ± 0.4 Ma (1s) (Gleadow et al., 2015)
Deep Creek	Eocene	Monzogranite	Deep Creek Range East-Central Nevada, USA	-113.92	39.83	A1, A2, B1, B2, C2	31	Zircon U-Pb 39 Ma ± 1 Ma (Rodgers, 1989); AHe 14.3-9.6 Ma* (TRaIL unpublished data)
Whitehorn	Cretaceous	Granodiorite	Arkansas Hills, Colorado, USA	-105.90	38.50	A1, A2, B1, B2	25	Zircon U-Pb 67.31 Ma + 0.57/-0.78 Ma (2s) (Abbey et al., 2017); Mean AHe 47.4 ± 4.2 Ma (1s) (Abbott et al., 2022)
McClure Mountain	Cambrian	Syenite	Wet Mountains, South-Central Colorado, USA	-105.47	38.35	A1, A2, B1, B2	36	Hornblende $^{40}Ar/^{39}Ar$ 523.2 ± 0.9 Ma (1s) (Spell and McDougall, 2003); AHe 150-70 Ma* (Weisberg et al., 2018)
Baileyville drill core	Proterozoic	Granite	Northeast Kansas, USA	-96.20	39.90	A1, A2, B1, B2	22	Zircon U-Pb ca. 1400 Ma (Van Schmus et al., 1987); AHe 150-70 Ma* (Flowers and Kelley, 2011)
Superior Craton	Archean	Tonalite	Superior Craton, Canada	-92.99	51.76	A1, A2, B1, B2	47	Zircon U-Pb 2720-2680 Ma (Hoffman, 1988); AHe 559 to 461 Ma* (TRaIL unpublished data)
Marlborough Fault System	Cretaceous	Sandstone	Kaikōura Ranges, South Island, New Zealand	173.69	−42.29	A1, A2, B1, B2, C1, C2	45	Deposition 100 ± 20 Ma (1s) (16MFS-05; Rattenbury et al., 2006), Mean AHe 4.2 ± 1.2 Ma (2s) (16MFS-05; Collett et al., 2019)
Marlborough Fault System	Cretaceous	Greywacke	Kaikōura Ranges, South Island, New Zealand	173.22	-41.78	B1, B2, C1, C2	30	Deposition 120 ± 22 (1s) (15MFS-07; Harbert, 2019; Mean AHe 5.4 ± 0.4 (2s) (15MFS-07; Harbert, 2019)

*** Range of single grain AHe dates from this sample**

[a] The number of grains for which high quality CT data were acquired. Not all grains in this dataset were included in the regressions; see Sect. 4.4.

Maximum width was used because for apatite it can be particularly difficult to measure the second width accurately. These lab analyses were subdivided into small (< 50 µm max width), medium (50-100 µm max width) and large (>100µm max width) size categories (shading in Fig. 2). From the samples described above we then picked suites of apatite crystals for CT with size distributions that were the same as that in the compiled datasets (Fig. 2). For apatite, the grains in our final dataset range in maximum width from 40 to 160 µm.

3.4 Selecting a Morphologically Representative Crystal Suite and Designing the Grain Evaluation Matrix

The morphology of the apatite grains used in this study encompass the spectrum of those regularly dated by (U-Th)/He. Prior to selecting grains for CT analysis, hundreds of apatite were inspected to gain a sense of the range of grain characteristics. These observations were then used to design a Grain Evaluation Matrix (GEM) (Fig. 3). This was done in part to evaluate whether specific grain qualities are associated with different systematic error or different uncertainty in the geometric parameters. The GEM provides a simple and reproducible method for categorizing the morphologic characteristics of apatite through which a single value (e.g., A1) succinctly describes the morphology of a crystal.

The GEM has two axes (Fig. 3): a “geometric classification” x-axis and a “roughness index” y-axis. Geometry and surface roughness were chosen for the GEM because apatite inspection revealed that these are the morphological features most likely to contribute to a grain’s deviation from the idealized hexagonal or elliptical geometry used to calculate 2D geometric parameters.

https://doi.org/10.5194/egusphere-2022-1005
Preprint. Discussion started: 18 October 2022

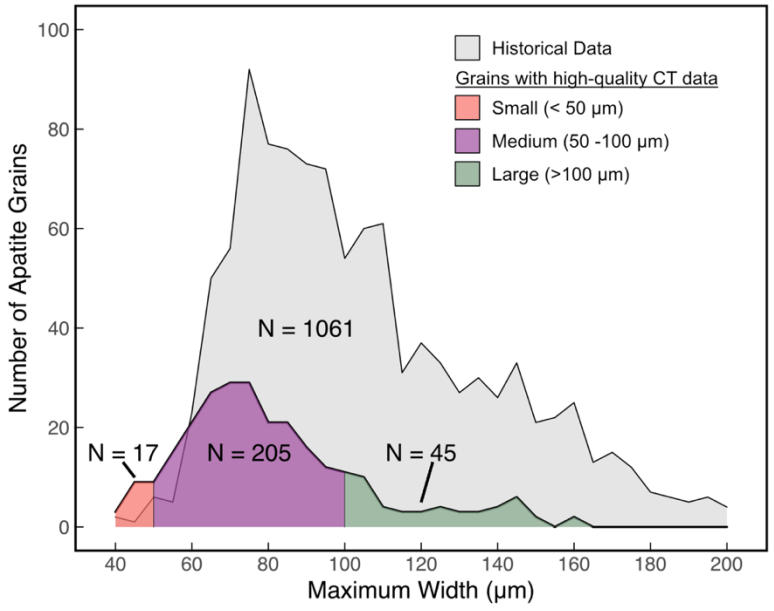

Figure 2. The distribution of maximum widths of apatite in this study. Light grey depicts 1061 apatite grains dated in the TRaIL between 2017-2019. Colored shading illustrates the size distribution of all grains for which we acquired high-quality CT data, with the number of grains in each size category listed. Note that not all grains shown here are included in the final regressions (for example, apatite grains with $F_T < 0.5$ were excluded from the regression analysis).

In the GEM, geometry is described as A (hexagonal), B (sub-hexagonal), or C (ellipsoid), where A and B grains assume a hexagonal geometry and C grains an ellipsoidal geometry for 2D calculations (Ketcham et al., 2011). Surface roughness is described as 1 (smooth) or 2 (rough).

Grains with missing terminations are sometimes analyzed by (U-Th)/He, so a subset of grains with one or two missing terminations was selected for CT analysis. For apatite, grains with missing terminations are approximately similar in proportion to those in the overall apatite sample suite.

For each apatite GEM category, grains from at least two samples and as many as eight samples were selected for CT analysis to ensure a range of subtle differences among grain types (Fig. B1). The number of grains selected for CT analysis in each GEM category was approximately proportional to the abundance of grains in that category in the entire sample suite. For example, because B1 (sub-hexagonal, smooth) apatite crystals were more common than C2 (ellipsoid, rough) crystals in the apatite suite, more B1 than C2 apatite were analyzed by CT.

Grain roughness (the y-axis of the GEM) was ultimately determined to have no bearing on the correction or uncertainties reported. Despite this, the GEM retains this axis because the GEM is a simple, coherent, and consistent tool for identifying and communicating grain characteristics that can influence the (U-Th)/He date. Noting the roughness of the apatite grain is useful for evaluating overall sample quality and can aid in identifying and evaluating dispersion in a (U-Th)/He dataset.

https://doi.org/10.5194/egusphere-2022-1005
Preprint. Discussion started: 18 October 2022

Additionally, the GEM is a useful teaching tool to show the wide variety of grain morphologies possible for apatite grains for newcomers to mineral picking.

4 Measurement and Data Reduction Methods

4.1 Strategy

The goals of this work are to develop corrections for systematic error and assign appropriate uncertainties to conventional "2D" microscopy estimates of the geometric parameters by comparing 2D values with "3D" values derived from CT data. To do this we first measured our suite of representative apatite crystals using the 2D microscopy approach (Sect. 4.2) and then acquired high-resolution (0.64 µm) CT data for these grains (Sect. 4.3). We then examined the 2D-3D relationships, linearly regressed them to determine corrections depending on grain geometry that make the 2D measurements as close to the 3D values as possible, and calculated uncertainties (Sect. 4.4). This analysis assumes that the 3D values are accurate. The final corrections and uncertainties are most appropriate for grains with characteristics like those used in this calibration study, with geometries like those in Figure 3, axial ratios < 1.7, maximum widths of 50-160 µm, and with microscopy measurements and 2D calculations done as described below. F_T uncertainties include only those uncertainties associated with grain geometry and not those due to parent isotope concentration uncertainties or zonation, grain abrasion, or crystal breakage.

4.2 Microscopy measurements and 2D calculation methods

Apatite grains were hand-picked under a Leica M165 binocular microscope under 160X magnification. Each grain was photographed on a Leica DMC5400 digital camera, manually measured using the Leica LAS 4.12 software, and a GEM value assigned (Fig. 3). The initial measurement procedure consisted of first measuring the long and short axes of each grain to obtain the grain's length and "maximum width", followed by rolling the grain 90° and again measuring the long and short axes to obtain a second length measurement and the grain's "minimum width". However, given the difficulty of measuring the minimum width accurately, we used the grain's length and maximum width to calculate the 2D values (Fig. 4; Appendix A).

We find a typical measurement uncertainty of 2.8 µm at 1s standard deviation. This was determined based on repeat measurements by 3 individuals of 258 apatite crystals. Each individual measured both lengths and the maximum width of each grain, for a total of 774 measurements per person. The 1s sample standard deviation for each grain dimension was calculated, with an average standard deviation of 2.8µm.

https://doi.org/10.5194/egusphere-2022-1005
Preprint. Discussion started: 18 October 2022

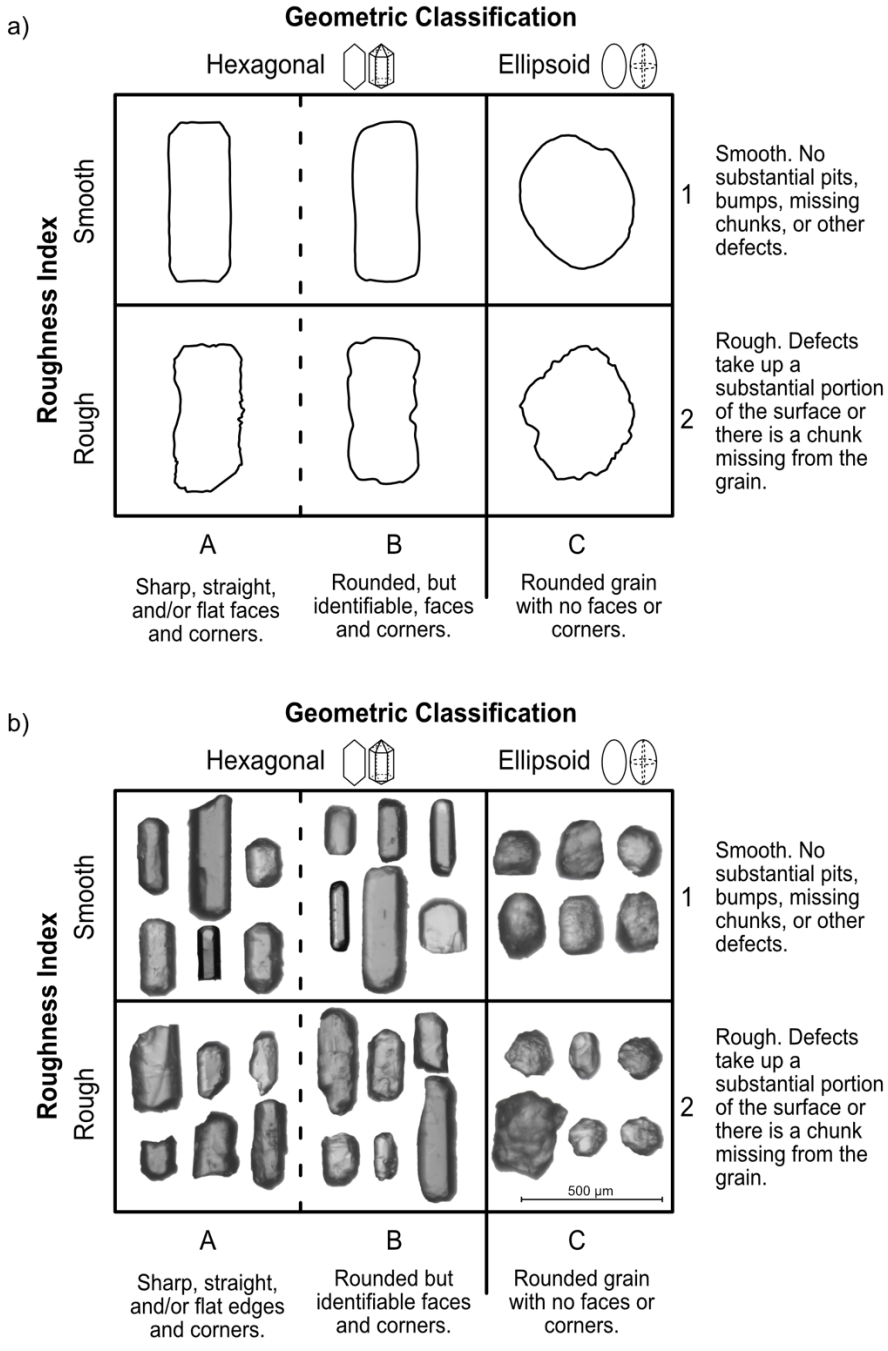

285

Figure 3. The apatite Grain Evaluation Matrix (GEM) in (a) schematic form and (b) with images of real grains analyzed in this study. The geometric axis classifies grains as A (hexagonal), B (sub-hexagonal), or C (ellipsoid). The roughness index classifies grains as 1 (smooth) or 2 (rough). Grains can be described by combining a geometric value and a roughness value (eg. A1, B2).

https://doi.org/10.5194/egusphere-2022-1005
Preprint. Discussion started: 18 October 2022

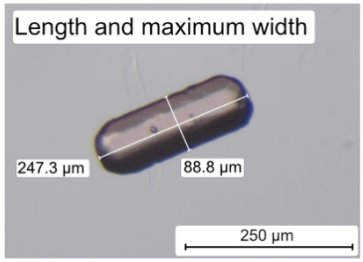

Figure 4. Photomicrograph of apatite grain showing how 2D microscopy measurements were acquired. The minimum width is measured after rolling the grain 90° onto its side after the first measurement is completed.

The 2D V values and the isotope-specific F_T values were calculated assuming the idealized geometries and equations in Ketcham et al. (2011). R_{FT} values were calculated using the equations in Cooperdock et al. (2019). We used the mean stopping distances for ^{238}U, ^{235}U, ^{232}Th and ^{147}Sm from Ketcham et al. (2011). The F_T calculations of Ketcham et al. (2011) assume that every surface is an ejection surface. All equations are listed in Appendix A. A hexagonal geometry was used for all A and B (hexagonal and sub-hexagonal) grains, while an elliptical geometry was used for all C (ellipsoid) grains. For each apatite, we calculated the R_{FT} value by assuming an apatite Th/U ratio of 1.94 and no contribution from Sm, where the Th/U ratio is the average of the TRaIL apatite sample historical data (N = 1061 grains) shown in Fig. 2. We made this assumption because the R_{FT} depends on the proportion of each parent isotope contributing to ^4He production, and we do not have parent isotope values for the grains analyzed by CT in this study.

4.3 Nano-computed tomography and 3D calculation methods

After 2D measurements, apatite grains were mounted for CT. Crystals were mounted in an ~600 x 600 µm area on a thin, 2000 µm wide plastic disc that was hole-punched from a plastic sheet protector and then covered with double sided tape (Fig. 5). Each plastic disc was constructed with a 0.025 mm diameter wire running down the center to act as a point of orientation to aid in the identification of grains post-scan. It was later discovered that the high-density wire created challenges for data reduction, so this approach is not recommended for future studies. Each plastic disc held 4-10 grains and 5-6 discs were stacked vertically to create a mount (Fig. 5). Mounts were secured by a thin layer of parafilm, attached to a 1-2 mm thick cylinder of rubber for stabilization, and then glued to the head of a flat-head pin (Fig. 5).

Each mount was scanned on a Zeiss Xradia 520 Versa X-ray Microscope in the University of Colorado Boulder Materials Instrumentation and Multimodal Imaging Core (MIMIC) Facility. Scanning parameters were optimized to reduce noise and scanning artifacts during test scans of the first mount. Scanning parameters were kept constant for subsequent mounts. All mounts were scanned with the 20X objective at relatively low power and voltages with small distances between the mount, source, and detector, which allowed for high resolution (0.64 µm). Table B1 reports the scan parameters.

https://doi.org/10.5194/egusphere-2022-1005
Preprint. Discussion started: 18 October 2022

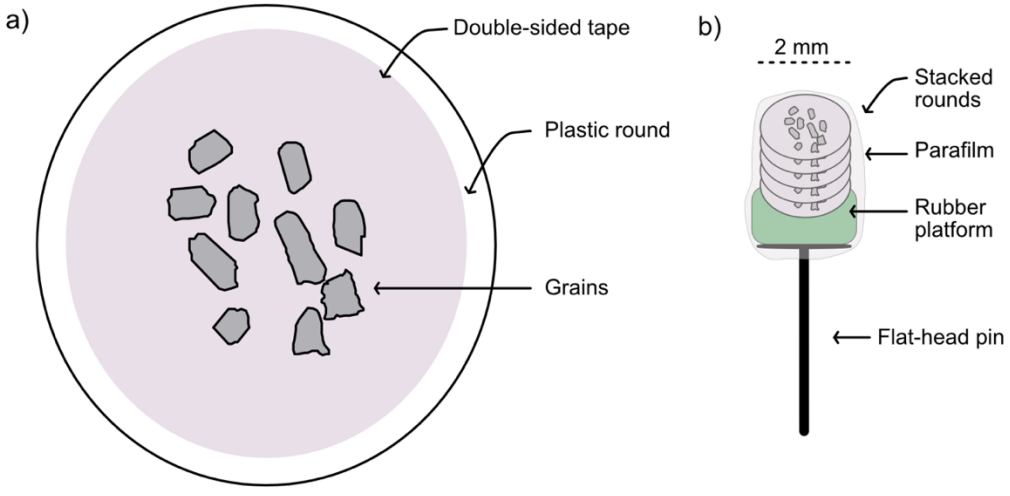

Figure 5. Schematic showing (a) an individual plastic round and (b) a final grain mount for CT analysis. The wire is not shown because it should not be included in future studies. Grains are placed onto a ~2mm wide sturdy plastic disc (hole punched from a plastic sheet protector) covered with double-sided tape. Each plastic round can hold between 4-10 grains. Rounds are stacked on top of each other and placed on a rubber platform cut from old test tube stoppers, which is glued to a flathead pin and covered with Parafilm.

Raw CT data were imported into Blob3D (Ketcham, 2005; freely distributed software) to calculate the dimensions, V, surface area, and isotope-specific F_T values for each grain. First, the grains were segmented, or separated, from the matrix, noise, and other grains, such that each grain was a separate 'blob' that had its V, surface area, and F_T values calculated. Segmentation was done with Dragonfly software, Version 2020.2 for Windows (Dragonfly, 2020) due to the complex nature of the artifacts arising from the use of the wire. After segmentation, final 3D parameters were calculated by Blob3D. Blob3D calculates V by counting the number of voxels (3D-pixel) in the segmented object and multiplying that number by the volume of each voxel. Blob3D calculates surface area by summing the faces of the isosurface surrounding the grain voxels and then smoothing it to reduce the effects of pixelation caused by the cubic voxels (Ketcham, 2005; Cooperdock et al., 2019). Blob3D calculates ^{238}U, ^{235}U, ^{232}Th, and ^{147}Sm F_T correction using a Monte Carlo approach that randomizes the starting location of an alpha particle within the selected volume of an object. The direction of ejection of the alpha particle is calculated via uniform sampling (Ketcham and Ryan, 2004). Blob3D uses stopping distances as reported in Ketcham et al., (2011) and assumes that ejection occurred across all surfaces. Like for 2D R_{FT} values, we calculated 3D R_{FT} values using the equations of Cooperdock et al. (2019) and assuming a Th/U ratio of 1.94 based on TRaIL apatite sample historical data.

Some data points were removed due to issues during CT scanning or subsequent data processing. Due to the use of the 20X objective for high resolution, many of the original 400 grains were lost because the edges of grains were 'cut off' during scanning. Additionally, the high-density wire in the apatite mounts introduced challenges for data reduction, like 3D models that had large holes or complex surface artifacts. This dataset consists of 267 apatite grains with high-quality CT data.

https://doi.org/10.5194/egusphere-2022-1005
Preprint. Discussion started: 18 October 2022

4.4 Statistical comparison of 2D and 3D values

The first step in our 2D-microscopy vs. 3D-CT data comparison was to generate scatter plots of 3D vs. 2D data for volume, isotope-specific F_T, and R_{FT} values (Fig. 6). We show only the isotope-specific ^{238}U F_T value for illustrative purposes because ^{238}U dominates the He production budget, but we treated the data for the ^{235}U, ^{232}Th, and ^{127}Sm isotope-specific F_T values in the same manner (Fig. C1). We did not examine surface area separately because although it is used together with volume to determine the F_T value, it is not alone used to calculate any other geometric parameter (unlike volume, which is used to calculate concentrations). We excluded from the plots and regressions the grains (N=28) with 2D and 3D F_T values <0.5, which are grains smaller than those typically analyzed by (U-Th)/He. This exclusion resulted in the elimination of all "small"-sized grains with <50 µm max width from the regressions. Overall, these small grains are characterized by greater differences between 2D and 3D values and higher scatter than the medium- and large- sized grains in our dataset, and we wanted to avoid biasing the corrections and uncertainties for the routinely dated apatite with data for atypically analyzed grains. The final regressed dataset has 237 apatite.

On the 3D versus 2D plots, if the data fall on the 1:1 line (bold black line), then no correction for systematic error is needed for the 2D data because the 2D data are in agreement with the 3D data. If the data fall off the 1:1 line, then the correction desired for the 2D data can be viewed as the offset of the data and its linear regression line from the 1:1 line. To determine corrections for systematic error, ordinary least squares linear regression with the intercept fixed at the origin was used. We explored several regression approaches, but ultimately chose an unweighted approach because the scatter of the 2D data that we wish to characterize includes both the uncertainty on the grain length and width measurements and other factors such as surface roughness and deviation from the assumed idealized grain geometry. We also explored fixing versus not fixing the y-intercept at (0,0). Here we present only the results of regressions with the y-intercept fixed at 0, because the unconstrained regressions generally yield intercepts within uncertainty of 0 and we would expect that if 2D measurement of any parameter was 0, then the 3D value would also be 0.

To evaluate if different groups of grains have statistically different slopes (and thus should have different corrections applied to them) we used Tukey's test (Table C1). Separate linear regressions were done for grains that use different geometric assumptions, so hexagonal apatite (A and B grains in Figure 3) were regressed separately from ellipsoid apatite (C grains in Figure 3). The slopes for the linear regressions of these two groups are statistically distinguishable, justifying their separation by geometry. Linear regressions were also done by grouping by surface roughness (1 vs 2 on the GEM, Figure 3) and size (medium, large). The linear regression slopes for these different categories are each statistically indistinguishable, indicating it is reasonable to only group the data by geometry for all parameters (Table C1).

The uncertainty for each 2D geometric parameter is the scatter of the points about the regression line. To determine the uncertainty of each 2D parameter, we calculated the 1s standard deviation of the residual values of all points from the regression line. This is shown on Figure 6 as plots of residual

https://doi.org/10.5194/egusphere-2022-1005
Preprint. Discussion started: 18 October 2022

percent difference versus maximum width for each parameter. To assess if physical parameters (e.g., roughness, size) are associated with patterns in these residuals, we compared the standard deviations for different groups of physical variables (Table C2).

The correlation of isotope-specific F_T uncertainties was also evaluated because we expect them to be highly correlated (Martin et al., in review). The correlation coefficient between each isotope-specific F_T was calculated using Pearson's R.

5 Results

5.1 Corrections for systematic error

The 3D versus 2D scatter plots for V, F_T, and R_{FT} (Figure 6A-C) all show data that systematically plot below the 1:1 line (bold black line), indicating that for all parameters the 2D values overestimate the "true" 3D values. The 2D data can be corrected for their systematic overestimation of the 3D data by multiplying the 2D data by the slope of the 3D vs. 2D data, so that the 2D data are centered around the 1:1 line, thereby "correcting" them. As noted above, regressions of the 3D vs. 2D data are separated by geometry because the regressions of hexagonal and ellipsoidal grains yield statistically distinguishable slopes.

The corrections for systematic error for apatite V, F_T, and R_{FT} are summarized in Table 2. For all parameters, the magnitude of the correction is smaller for hexagonal grains than for ellipsoid grains. For example, for V, the slope of the regression line is 0.83 for hexagonal grains and 0.74 for ellipsoid grains. This means that the volumes estimated by microscopy measurements typically overestimate the true grain volume by 17% for hexagonal grains, and by 26% for ellipsoid grains. For $^{238}F_T$, the corrections are substantially smaller, with values of 0.97 and 0.92 for hexagonal and ellipsoid grains. For R_{FT}, the corrections are 0.93 and 0.85 for hexagonal and ellipsoid grains.

5.2 Uncertainties

The uncertainties for V, F_T, and R_{FT} are derived from the scatterplots of the percent difference in the residuals versus maximum width in Figure 6D-F, where the bold black line represents no difference between the 2D and 3D data. The uncertainties are grouped by geometry for all parameters, because the residuals are derived from the regression lines, which group data in this way. The standard deviation of the percent difference in the residuals of each group is the uncertainty on the parameter, which are reported in Table 2 at 1s. A single uncertainty is reported for ellipsoid apatite grains for all parameters due to the relatively small number of ellipsoid grains in the dataset (N = 36). However, for hexagonal grains, the data population (N= 201) is large enough that we explored surface roughness and grain size as potential grouping variables. We did not find a consistent, substantial relationship between surface

https://doi.org/10.5194/egusphere-2022-1005
Preprint. Discussion started: 18 October 2022

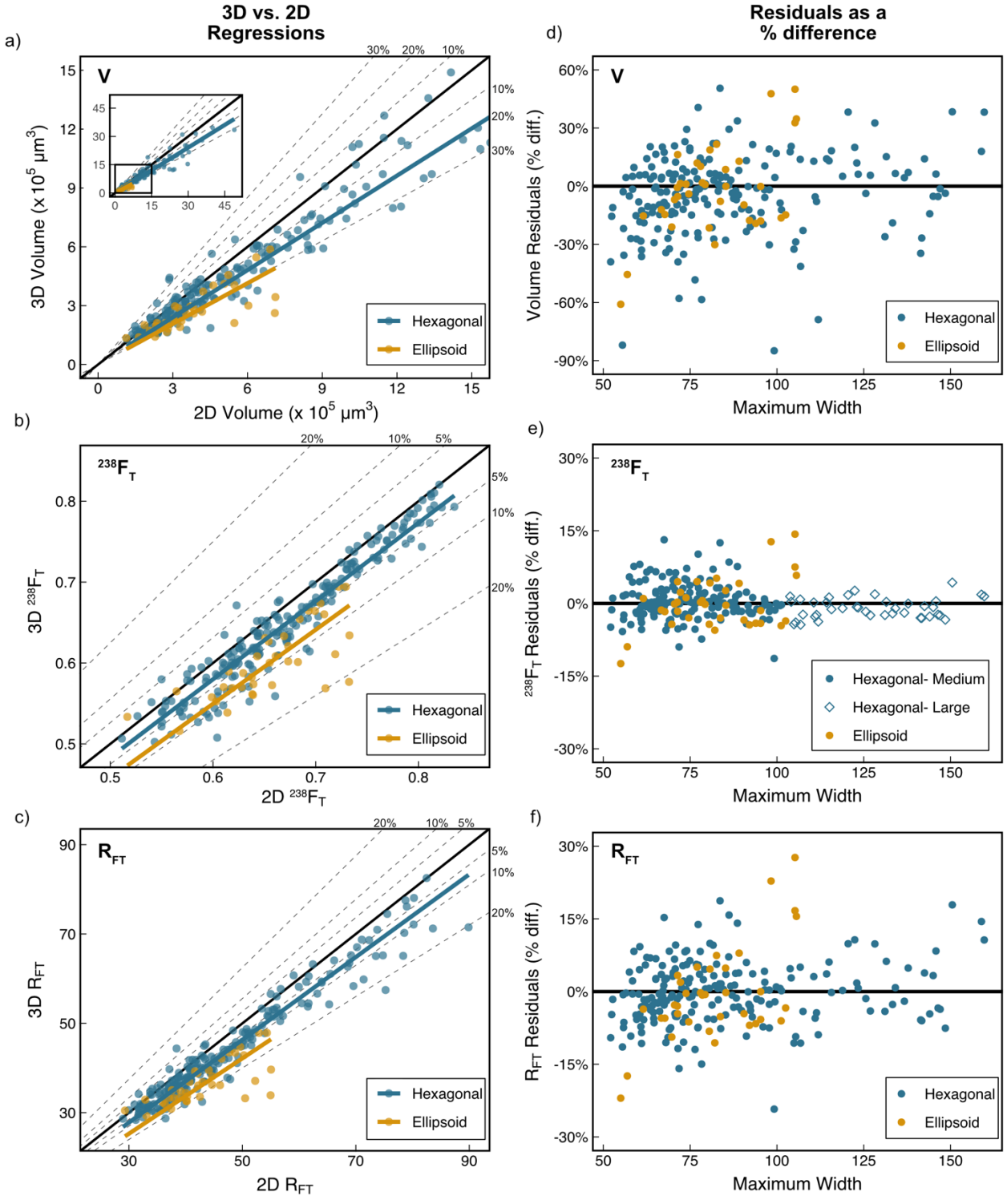

https://doi.org/10.5194/egusphere-2022-1005
Preprint. Discussion started: 18 October 2022

Figure 6. These plots illustrate how the corrections for systematic error and how uncertainties were determined for V, F_T, and R_{FT}. Scatter plots of 3D vs. 2D data (N=237) with regression lines and data distinguished by geometry for (a) V, (b) $^{238}F_T$, and (c) R_{FT}. Grains with $F_T < 0.5$ were excluded from the regressions. The bold black line is the 1:1 line and the dashed lines mark the percent difference from the 1:1 line. Note that for all regressions, the regression line falls below the 1:1 line, indicating that the 2D-microscopy data overestimate the 3D-CT data. The 2D data can be corrected for systematic error by multiplying the 2D data by the 3D/2D slope. Plots of the difference of each 2D value from the regression line (i.e., the residual) as a percent difference vs. maximum width with data distinguished by geometry for (d) V, (e) $^{238}F_T$, and (f) R_{FT}. For $^{238}F_T$ the hexagonal grains are additionally split by medium (50-100 µm maximum width) vs. large (> 100 µm maximum width) size. The bold black line is 0% difference. Note the larger y-axis scale for V as compared with $^{238}F_T$ and R_{FT}, reflecting the greater uncertainty of V. The standard deviation of the % difference in the residuals of each group is the uncertainty on the parameter.

roughness and uncertainty in the data (Table C2). However, for grain size, the $^{238}F_T$ uncertainty for medium-sized (maximum width 50-100 µm) hexagonal apatite is greater than for large-sized (maximum width > 100 µm) hexagonal apatite. As described below, this pattern is sensible, so we report two uncertainties for the isotope-specific F_T values of hexagonal grains based on size.

For all parameters, the uncertainty for hexagonal grains is smaller than the uncertainty for ellipsoid grains (Table 2). For V, the uncertainty is 20% for hexagonal grains and 23% for ellipsoid grains of all sizes. For $^{238}F_T$, the uncertainties are 3% and 2% for medium and large hexagonal grains, respectively, and 5% for all ellipsoid crystals. For R_{FT}, the uncertainty is 6% for hexagonal grains and 10% for all ellipsoid grains of all sizes.

As anticipated, the isotope-specific F_T uncertainties are highly correlated, yielding values of 0.972-0.999. For this reason, below we assume fully correlated uncertainties of 1 for F_T uncertainty propagation into the corrected date.

6 Discussion

6.1. Grain characteristics that influence the accuracy and precision of 2D geometric data

The goal of this study was to develop a simple method for correcting for systematic error and for assigning uncertainties to geometric parameters estimated from microscopy measurements for the full spectrum of apatite crystals that are regularly analyzed by (U-Th)/He. Thus, the corrections for systematic error are intended to improve the accuracy of the V, F_T, and R_{FT} values derived from 2D data. The uncertainties are aimed at appropriately representing the reproducibility or precision of these geometric parameters. Accomplishing this required determining the grain characteristics that most affect the accuracy and precision of the 2D data.

We find that the magnitude of the systematic error is influenced primarily by the first-order grain morphology. For example, whether apatite grains are hexagonal or sub-hexagonal (A or B on the GEM) vs. ellipsoid (C on the GEM), dictates the choice of a hexagonal or ellipsoid idealized geometry. This in turn determines the magnitude of the correction required to make the geometric parameters calculated from the microscopy data accurate (e.g., for $^{238}F_T$ a 0.97 correction for hexagonal grains vs. a 0.92 correction for ellipsoid grains).

https://doi.org/10.5194/egusphere-2022-1005
Preprint. Discussion started: 18 October 2022

Table 2. Corrections and uncertainties (1s) for all geometric parameters.

Volume

Geometry	Correction[a]	% Uncert.[b] (1s) for apatite grains of all sizes
Volume		
Hex.	0.83	20%
Ellip.	0.74	23%

Isotope-specific F_T values

Geometry	Correction	% Uncert. (1s) for medium-sized[c] apatite grains	% Uncert. (1s) for large-sized[d] apatite grains
$^{238}F_T$			
Hex.	0.97	3%	2%
Ellip.	0.92	5%	5%
$^{235}F_T$			
Hex.	0.96	4%	2%
Ellip.	0.91	6%	6%
$^{232}F_T$			
Hex.	0.96	4%	2%
Ellip.	0.91	6%	6%
$^{147}F_T$			
Hex.	0.99	1%	1%
Ellip.	0.97	1%	1%

R_{FT}

Geometry	Correction	% Uncert. (1s) for apatite grains of all sizes
R_{FT}		
Hex.	0.93	6%
Ellip.	0.85	10%

[a] **The correction value is the slope of the 3D vs. 2D regression line for each parameter in Figures 6A-6C.**

[b] **The uncertainty is the scatter of the 2D data about each regression line in Fig. 6A-C, calculated as the 1s standard deviation of the % difference of each 2D value from the regression line (Fig. 6D-F).**

[c] **"Medium-sized" apatite have maximum widths of 50-100 µm.**

[d] **"Large-sized" apatite have maximum widths of >100 µm.**

https://doi.org/10.5194/egusphere-2022-1005
Preprint. Discussion started: 18 October 2022

Our results show that the uncertainty in the 2D geometric parameters is controlled primarily by the grain geometry, and for F_T, secondarily by the grain size. Uncertainties on hexagonal grains are consistently smaller than those for ellipsoid grains (Table 2). For example, for V, uncertainties are 20% and 23% for hexagonal and ellipsoid grains. For R_{FT}, these uncertainties on hexagonal grains are again smaller (6%) than for ellipsoid grains (10%). For $^{238}F_T$, grain size exerts additional influence on the uncertainty of hexagonal grains, with uncertainties of 3% and 2% for grains with maximum widths of 50-100 µm and > 100 µm, respectively, compared with an uncertainty of 5% for ellipsoid grains of all sizes. The influence of size on the F_T uncertainty is not surprising given that the effect of the uncertainty in grain measurements (± 2.7 µm) is proportionately larger for smaller grains. This pattern is consistent with early work that estimated F_T uncertainty decreased with increasing grain size (Ehlers and Farley, 2003).

6.2 Overestimation of the 3D geometric parameter values by the 2D microscopy method

6.2.1. Overview

In this study, all values calculated from the 2D microscopy measurements overestimate the real 3D values. This is true regardless of grain size, morphology, and other grain characteristics. Compared with past work (Herman et al., 2007; Evans et al., 2008; Glotzbach et al., 2019; Cooperdock et al., 2019), in this study we analyzed more apatite (237 compared with 4-109) and at a higher CT resolution (0.64 µm compared with 1.2 -6.3 µm). We also deliberately included the full variety of grain morphologies across a range of grain sizes from samples of variable age and lithology, so we have confidence that the results are applicable to the spectrum of routinely analyzed crystals.

As explained in Sect. 4.4, the corrections and uncertainties discussed above and reported in Table 2 are calculated from the regressions and are computed in this way because the objective of our work is to systematically correct real 2D data and routinely apply the associated uncertainty to them. However, previous studies, which did not have these same goals in mind, reported the average 3D/2D value and its 1s uncertainty as a measure of systematic error, and reported the average absolute percent difference between the 2D and 3D data and its 1s uncertainty as a measure of the uncertainty of each parameter. To directly compare our results to this past work, in Table 3 we also report our results in this way. This table directly follows the structure of Table 3 in Cooperdock et al. (2019). In our Table 3, we report values for our entire dataset, as well as subdivided by hexagonal and ellipsoid geometry. However, for simplicity, we use only the average values for our whole dataset in the discussion below.

We place our results in the context of those of Cooperdock et al. (2019) and Glotzbach et al. (2019) because these two studies directly compared 2D microscopy with 3D CT values for a moderate to large suite of apatite crystals. Cooperdock et al., (2019) characterized 109 hexagonal to sub-hexagonal apatite grains (A1 and B1 in our GEM) by CT (5 µm resolution), while Glotzbach et al. (2019) analyzed 24 apatite crystals (1.2 µm CT resolution) with a wider range of characteristics (rounded through euhedral morphologies).

https://doi.org/10.5194/egusphere-2022-1005
Preprint. Discussion started: 18 October 2022

Table 3. 2D microscopy and 3D CT data comparison for this and previous studies[a]

This Study: 237 apatite grains; CT resolution: 0.64 µm				
	avg. 3D/2D[b]	1s	abs. avg. % diff.[c]	1s
All data: 237 grains				
Volume	0.85	0.17	19	13
$^{238}F_T$	0.96	0.04	4	4
R_{FT}	0.92	0.07	8	6
Hexagonal apatite: 201 grains				
Volume	0.87	0.17	18	12
$^{238}F_T$	0.97	0.03	4	3
R_{FT}	0.93	0.06	7	5
Ellipsoid apatite: 36 grains				
Volume	0.75	0.17	26	15
$^{238}F_T$	0.92	0.05	8	4
R_{FT}	0.86	0.08	15	8

Previous Studies				
	avg. 3D/2D	1s	abs. avg. % diff.	1s
Cooperdock et al. (2019): 108 apatite grains; CT resolution: 4-5 µm				
Volume	0.82	0.22	23	16
$^{238}F_T$	1.01	0.02	2	2
R_{FT}	1.02	0.07	5	5
Glotzbach et al. (2019): 24 apatite grains; CT resolution: 1.2 µm				
Volume	1.04	0.2	15	13
$^{238}F_T$	0.99	0.02	2	2
R_{SV}[d]	0.93	0.06	8	5

[a] Directly follows the structure of Table 3 reported in Cooperdock et al. (2019) to facilitate comparison with previous studies.

[b] avg. 3D/2D is the average of all 3D/2D values in each study

[c] abs. avg. % diff. Is the average absolute percent difference between the 2D and 3D data. We used the formula $\left(\frac{|2D-3D|}{2D}\right) \times 100$ to calculate the percent difference for consistency with Cooperdock et al. (2019).

[d] Glotzbach et al. (2019) reports R_{SV} rather than R_{FT}.

Although Evans et al. (2008) also carried out a study of this kind and was the first to do this type of comparison, that work included only four apatite crystals (3.8 µm CT resolution). Herman et al. (2007) used CT to derive geometric parameter data for 11 detrital apatite grains (6.3 µm CT resolution) but did not compare the results with 2D microcopy estimates for the same grains.

https://doi.org/10.5194/egusphere-2022-1005
Preprint. Discussion started: 18 October 2022

6.2.2. Volume

Of the geometric parameters evaluated in this study, V shows the greatest overestimate of 2D relative to 3D values (2D value corrections of 0.83 and 0.74 depending on geometry) and the greatest data scatter (20% and 23%) (based on the data regressions, Table 2). If we instead report our outcomes as the average 3D/2D value and the average absolute % difference, we obtain values of 0.85 and 19% for all grains (Table 3). This result is generally consistent with those of previous work. Cooperdock et al., (2019) found an average 3D/2D value of 0.82 and an average difference of 23%. Glotzbach et al. (2019) found no systematic over- or underestimate in volume (avg 3D/2D = 1.04) but a similar magnitude of variation (15%).

6.2.3. F_T

For F_T, our 2D values overestimate the 3D values. The isotope-specific $^{238}F_T$ has a 2D correction value of 0.97 for hexagonal grains and 0.92 for ellipsoid grains, with uncertainties of 2-5% depending on geometry and size (based on the regressions, Table 2). The corrections and uncertainties for the other isotope-specific F_T values vary from 0.99 to 0.91 and 1-6% (again depending on grain geometry and size, Table 2), but we again focus on the $^{238}F_T$ value here because it dominates the ^{4}He production. Our average 3D/2D value for $^{238}F_T$ is 0.96, with an average difference of 4% (Table 3). This outcome is similar to that of Glotzbach et al. (2019) (avg. 3D/2D = 0.99; avg. abs. diff. = 2%). In contrast, Cooperdock et al. (2019), report 2D values that slightly underestimate the 3D F_T values (average 3D/2D = 1.01), but with a comparable magnitude of scatter (2%). This may be due, in part, to their grain selection, which focused mainly on high quality, hexagonal apatite grains.

6.2.4. R_{FT}

For R_{FT}, we found that 2D measurements were systematically larger than 3D measurements (2D correction values of 0.93 and 0.85), with uncertainties of 6-10% depending on geometry (based on the regressions, Table 2). Our average 3D/2D value for R_{FT} is 0.92, with an average difference of 8% (Table 3). Glotzbach et al. (2019) reports R_{SV} (the equivalent sphere with the same surface area to volume ratio as the grain) rather than R_{FT}, but these values typically have little to negligible difference. Their dataset yields R_{SV} outcomes nearly identical to our R_{FT} results (avg. 3D/2D = 0.93; avg. abs. diff. = 8%). In contrast, Cooperdock et al. (2019) found an average 3D/2D value of 1.02 and an average difference of 5% (Table 3). Their underestimation of R_{FT} by 2D measurements is expected given the systematic underestimation they report for F_T.

6.3 Implications: How much do the corrections and geometric uncertainties matter?

6.3.1 Overview

To determine how much the corrections and geometric uncertainties (Table 2) affect the values and uncertainties on real (U-Th)/He dates and other key parameters, we apply our corrections and uncertainties to the V, F_T, and R_{FT} values of a subset of representative apatite grains from three samples

https://doi.org/10.5194/egusphere-2022-1005
Preprint. Discussion started: 18 October 2022

(N=24) that were used in this study and that were previously dated in the CU TRaIL (Table D1). This apatite suite includes both hexagonal and ellipsoid grains with a range of sizes. We then use the corrected V and isotope-specific F_T values to calculate the parameters derived from them—mass, eU, and the corrected (U-Th)/He date—and propagate the geometric uncertainties on V and F_T into the uncertainties of the derived values. Below, we then compare the "new" values and uncertainties on all parameters with their "original" uncorrected counterparts (Sect. 6.3.2-6.3.5), generate corrected apatite (U-Th)/He (AHe) date vs. eU plots using both the new and original values (Fig. 7), and consider the broader implications of these outcomes for interpretation of AHe data (Sect. 6.3.6).

Table 4 summarizes the average new/original values for this example dataset, as well as how much the uncertainty on each parameter increases owing to the inclusion of geometric uncertainties (which have traditionally been excluded from the uncertainties reported on these parameters). For uncertainty propagation into the corrected (U-Th)/He date, we use HeCalc (Martin et al., in review) and assume fully-correlated (r = 1) isotope-specific F_T uncertainties. In Table 4 and the discussion below all uncertainties are reported at 1s. Standard practice in the CU TRaIL over the last several years has been to report 15% 1s uncertainties on eU based on estimates by Baughman et al. (2017). However, how eU uncertainties are reported varies widely across the community and it is common for no uncertainty to be reported on eU data, therefore for comparative purposes, no uncertainty is shown on eU_{orig} in Fig. 7A-C and none is reported in Table D1.

6.3.2 Mass and eU

To calculate eU, absolute quantities of U, Th, and Sm must be converted to concentrations using the apatite grain mass, which is computed from V assuming an apatite density (here we use 3.20 g/cm^3). Absolute amounts of parent isotope carry an analytical uncertainty, but conventionally the grain mass reported by labs has had no uncertainty attached to it because the geometric uncertainty on V (and therefore on mass) was not well constrained. By applying a correction factor to V based on grain geometry (0.83 or 0.74) and calculating mass using the corrected V, the $mass_{new}$ decreases by the same correction factor as volume. The mass then inherits the same percent uncertainty as volume (20 or 23%, 1s, depending on geometry).

For eU, the smaller $mass_{new}$ values (relative to $mass_{orig}$) are translated into larger eU_{new} values (relative to eU_{orig}). In our example dataset (Table 4), the average eU_{new}/eU_{orig} is 1.2 for hexagonal grains and 1.4 for ellipsoid grains. We propagated the analytical uncertainties on the parent isotopes only, as well as the analytical and geometric uncertainties, into the eU_{new} values. Propagating analytical uncertainties only yields average eU uncertainty values of 3% for hexagonal and ellipsoid grains in this dataset (with a range from 1 to 6%). Including both analytical and geometric uncertainties yields average uncertainties of 15% and 16% for hexagonal and ellipsoid grains (varying from 14-17%).

https://doi.org/10.5194/egusphere-2022-1005
Preprint. Discussion started: 18 October 2022

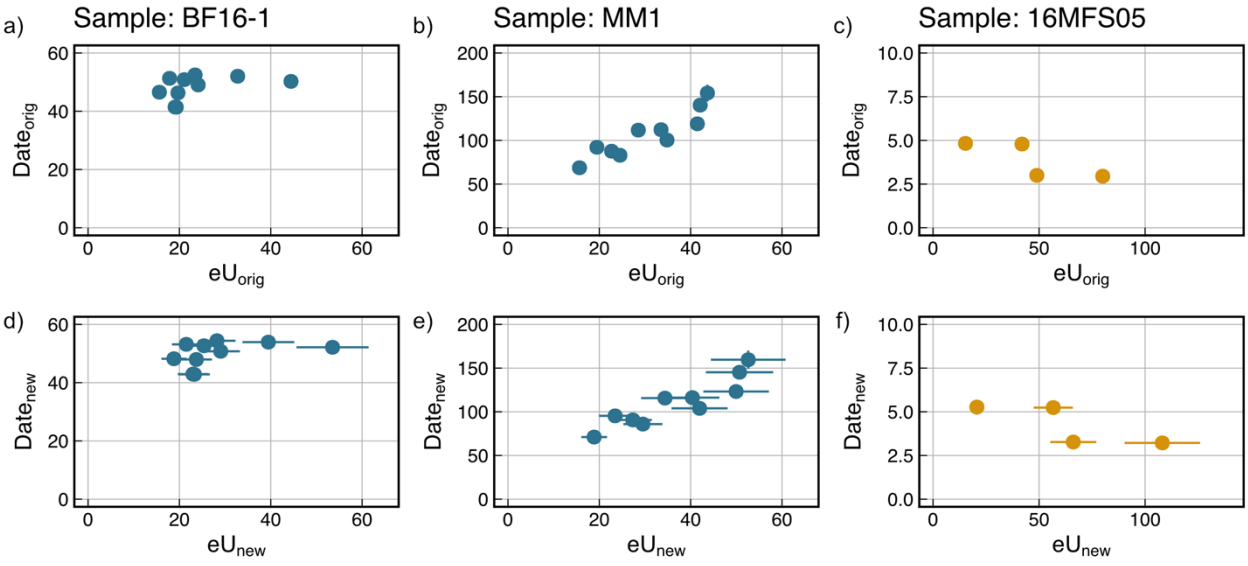

Figure 7. Date-eU plots for three samples previously dated in the CU TRaIL showing the effects of corrections and uncertainty estimates on typical AHe data. (a)-(c) are $date_{orig}$ vs. eU_{orig} plots, while (d)-(f) are $date_{new}$ vs. eU_{new} plots. When uncertainty bars are not visible they are on the order of the symbol size, except for the top row where no eU uncertainty is plotted.

6.3.3 Combined F_T values

The combined F_T values are calculated using both the isotope-specific F_T values and the amount of the parent isotopes, because the proportion of the parent isotopes dictates the proportion of the ^{4}He atoms that travel different mean stopping distances. The combined F_T values are not used for any additional calculations except R_{FT}, but are typically reported in data tables (e.g., Flowers et al., 2022a). For our example dataset, we apply the correction factors in Table 2 based on grain geometry and size to the isotope-specific F_T values, and then use these corrected values to calculate the combined $F_{T,new}$ value. $F_{T,new}$ is always smaller than $F_{T,orig}$ ($F_{T,new}$ / $F_{T,orig}$ = 0.97 and 0.92 for hexagonal and ellipsoid grains; Table 4).

F_T values have not typically been reported with an uncertainty, because until now the geometric uncertainty on F_T has been poorly quantified. We propagated uncertainties into the combined F_T value using the analytical uncertainties only, as well as using both analytical and geometric uncertainties. For the example dataset, inclusion of analytical uncertainties only yields average uncertainties on the combined F_T of 1% (1s, with a range from 0-3%) for both grain geometries. The propagation of both analytical and geometric uncertainties generates average values of 2% for hexagonal grains (varying from 1-3%) and 4% for all ellipsoid grains (Table 4). Variability in the uncertainties for the combined F_T is due to variability in the total analytical uncertainty.

https://doi.org/10.5194/egusphere-2022-1005
Preprint. Discussion started: 18 October 2022

Table 4. The average percent difference between the original and new values for example dataset of Table D1.

Parameter and Geometry[a]	Avg. New/Orig.[b]	% Uncertainty: Avg. analyt. uncert. only[c] (%), 1s	Min (%)	Max (%)	Avg. analyt. + geom. uncert.[d] (%), 1s	Min (%)	Max (%)	Avg. % uncert. increase[e], 1s
Mass								
Hex.	0.83	NA	NA	NA	20%	20%	20%	NA
Ellip.	0.74	NA	NA	NA	23%	23%	23%	NA
eU								
Hex.	1.20	3%	1%	6%	15%	14%	16%	12%
Ellip.	1.40	3%	2%	3%	16%	16%	17%	13%
Combined F_T								
Hex.	0.97	1%	0%	3%	2%	1%	3%	1%
Ellip.	0.92	1%	1%	1%	4%	4%	4%	3%
Corr. Date								
Hex.	1.04	2%	1%	6%	3%	2%	7%	1%
Ellip.	1.09	4%	2%	6%	7%	6%	8%	3%
R_{FT}								
Hex.	0.93	NA	NA	NA	6%	6%	6%	NA
Ellip.	0.85	NA	NA	NA	10%	10%	10%	NA

NA indicates "Not Applicable", for example, mass doesn't have any analytical uncertainty on the parent isotopes.

[a] There are N = 20 hexagonal and N = 4 ellipsoid grains.

[b] The average of the new parameter (calculated using the new values) divided by the average of the original values (calculated using the original values) for the example data in Table D1. Values under 1 indicate that the original value is larger than the new. Values over 1 indicate that the original value is smaller than the new.

[c] The average of the percent analytical uncertainties only for the example data in Table D1.

[d] The average of the percent analytical + geometric uncertainties for the example data in Table D1.

[e] The average percent increase is the difference between the analytical only and analytical + geometric uncertainties.

6.3.4 Corrected (U-Th)/He dates

The most rigorous means of calculating F_T-corrected (U-Th)/He dates is by incorporating the isotope-specific F_T corrections into the age equation and calculating the corrected date iteratively (Ketcham et al., 2011). For our example dataset, we used the corrected isotope-specific F_T values (as described above) to calculate the F_T-corrected AHe $date_{new}$. For the AHe dates, the smaller $F_{T,new}$ values (relative to $F_{T,orig}$) are translated into larger corrections for alpha-ejection. Thus, the $date_{new}$ values are always older than the $date_{orig}$ values (avg. $date_{new}$ / $date_{orig}$ = 1.04 and 1.09 for hexagonal and ellipsoid grains).

We calculated the uncertainty on the corrected (U-Th)/He dates in two ways for comparative purposes: first by propagating the analytical uncertainties on the parent and daughter only, and next by additionally including the geometric uncertainties on the isotope-specific $F_{T,new}$ values and assuming

https://doi.org/10.5194/egusphere-2022-1005
Preprint. Discussion started: 18 October 2022

fully-correlated $F_{T,new}$ uncertainties (Table 3). For this dataset, we find that propagating only analytical uncertainties yields average uncertainties of 2% and 4% for hexagonal and ellipsoid grains (varying from 1-6% and 2-6%, respectively). Including both analytical and geometric uncertainties yields average uncertainties of 3% and 7% for the two geometries (with 2-7% and 6-8% variability). The difference in the uncertainty on the date varies so widely because it is dependent on a variety of grain-specific factors—the absolute amounts of U, Th, Sm, and He, as well as grain geometry and size.

6.3.5 R_{FT}

We applied the correction factors based on grain geometry in Table 2 to R_{FT} values from the example dataset. The $R_{FT,new}$ values are always smaller than $R_{FT,orig}$ values ($R_{FT,new}$ / $R_{FT,orig}$ = 0.93 and 0.85 for hexagonal and ellipsoid grains) (Table 4). The uncertainty on R_{FT} is 6% (1s) for hexagonal grains and 10% (1s) for ellipsoid grains. This parameter is not used in the calculation of (U-Th)/He dates, but the uncertainty should be used during thermal history modeling when possible.

6.3.6 Summary

This exercise in which we both 1) correct real AHe data for systematic error associated with the 2D microscopy approach for determining geometric parameters, and 2) propagate geometric uncertainties into the uncertainties on eU and corrected AHe dates reveals a substantial influence of both on some aspects of the results. The most striking outcome is the impact on eU. For example, the eU_{new} values of the example dataset increase by 20-40%, resulting in a noticeable shift of data to the right on the date-eU plots (compare Fig. 7A-C with Fig. 7D-F). Moreover, the eU uncertainties when both analytical and geometric uncertainties are included are as much as 17% at 1s, indicating the importance of appropriately reporting and representing eU uncertainties. The influence of systematic error and uncertainties are less substantial for the corrected AHe date than for eU but, are still important. For ellipsoid grains, the AHe $date_{new}$ values are as much as 9% older than the $date_{orig}$ values, with typical uncertainties that increase by as much as 3% when geometric uncertainties are propagated in addition to analytical uncertainties. For hexagonal grains, the corrections and uncertainties are less than for ellipsoid grains, but non-negligible. Including the geometric uncertainty on the corrected AHe dates may help account for overdispersion in some (U-Th)/He datasets. We contend that properly correcting for systematic error and propagating uncertainties associated with the geometric parameters is an important step for rigorously presenting and interpreting apatite (U-Th)/He data.

6.4 The Geometric Correction Method: A practical workflow

The Geometric Correction Method described here and shown in Fig. 8 can be easily integrated into existing (U-Th)/He dating workflows with no additional time, cost, or equipment. This method assumes that grain characteristics are like those in this calibration study, with 2D microscopy F_T values > 0.5 and axial ratios < 1.7. It also assumes that grain measurements are made in the same manner as this study (Fig. 4) and that 2D V, F_T, and R_{FT} values are calculated using the equations of Ketcham et al. (2011) and Cooperdock et al. (2019). All equations required for the calculations below are in Appendix A. The corrections for systematic error and the uncertainties reported here are only those associated with grain

https://doi.org/10.5194/egusphere-2022-1005
Preprint. Discussion started: 18 October 2022

geometry. For F_T, additional inaccuracy and uncertainty may be introduced by parent isotope zonation, grain abrasion, and grain breakage, which have potential to be accounted for separately. For mass and the derived eU concentration, additional uncertainty may be associated with the assumed mineral density.

Step 1. Select grain geometry and GEM category. Choose apatite crystal for analysis. Decide whether the grain is hexagonal or ellipsoid, which is all that is strictly required to correct the 2D values and assign uncertainty. However, we strongly encourage assigning a GEM category (Fig. 3) and making other descriptive notes, which can be helpful for data interpretation.

Step 2. Measure the grain. Measure the grain using the procedure outlined in Sect. 4.2 and Figure 4.

- Measure the apatite grain's maximum width.
- Measure the grain length. Only a single length is required, however, if the grain has an extremely angled or uneven end then two lengths may be measured and their average reported to better capture the average length.

Step 3. Calculate the 2D values. Calculate 2D microscopy V and F_T values using the hexagonal or ellipsoid equations of Ketcham et al. (2011) depending on grain geometry. Calculate R_{FT} using the equations of Cooperdock et al. (2019).

Step 4. Correct the 2D values. Multiply the 2D microscopy V, isotope-specific F_T, and R_{FT} values by the correction according to the grain geometry to produce the V_{new}, $F_{T,new}$, and $R_{FT,new}$ values (Table 2). Typically, combined F_T values are reported by labs, but the isotope-specific F_T values are required for the most accurate and rigorous calculation of corrected (U-Th)/He dates (Ketcham et al., 2011)

Step 5. Assign uncertainty. Attach the uncertainty value to each parameter according to the grain geometry (for V_{new}, $F_{T,\,new}$, $R_{FT,\,new}$) and maximum width (for $F_{T,\,new}$) (Table 2).

Step 6. Calculate derived parameters and propagate uncertainties.

- Calculate mass and eU using the V_{new} values. Uncertainty on V should be propagated into the uncertainty on these derived parameters.
- Calculate corrected (U-Th)/He dates using the isotope-specific $F_{T,new}$ values. Uncertainty on F_T should be propagated into the final uncertainty on the corrected He date. This uncertainty propagation can be easily accomplished, for example, by using the open access Python program HeCalc for (U-Th)/He data reduction (Martin et al., in review).

Consider the following example: an apatite grain selected for analysis has a maximum width of 98 µm and a GEM value of B1. The $^{238}F_{T,orig}$ of this grain is 0.67 (see Appendix A and the footnotes of Table D1 for the details of this calculation). The analyst uses Table 2 to select the correction for hexagonal grains (0.97) and performs the following calculation:

$$F_{T,\,new} = F_{T,orig} \times \text{correction} = 0.67 \times 0.97 = 0.65$$

https://doi.org/10.5194/egusphere-2022-1005
Preprint. Discussion started: 18 October 2022

The analyst then selects the proper uncertainty from Table 2 based on grain geometry and maximum width. This hexagonal grain is considered medium-sized because it is 98 µm wide, so it has an uncertainty of 3%. The final $^{238}F_{T, new} = 0.65 \pm 3\%$. This procedure is repeated for each isotope-specific $F_{T, orig}$. The isotope-specific $F_{T, new}$ values are used in the calculation of the corrected date and both the uncertainty on each isotope-specific F_T and the analytical uncertainty is propagated into the uncertainty on the corrected (U-Th)/He date.

7 Conclusions

Uncertainties on the geometric parameters and the data derived from them – V, F_T, R_{FT}, eU, and corrected (U-Th)/He dates – have not traditionally been included in the reported uncertainties on (U-Th)/He datasets. Nor have such data been corrected for systematic error that might arise from the 2D microscopy approach for determining these values. Although both uncertainties and corrections are important for accurate interpretation of (U-Th)/He datasets, the lack of well-quantified values that can easily be determined and applied to routinely generated data has hindered progress in this area.

In this paper we present the only no-cost, easy-to-implement, and backwards-compatible solution to this problem. The Geometric Correction Method is a simple and effective set of corrections and uncertainties derived for V, F_T, and R_{FT} values that can be easily incorporated into existing workflows (Fig. 8). This approach corrects these parameters for systematic overestimation and provides an uncertainty that can be propagated into the uncertainty on derived parameters (eU, corrected date). It also can be easily applied to previously published data.

We also present the Grain Evaluation Matrix (GEM), which is a simple, clear, and consistent method to systematically characterize apatite grain quality (Fig. 3). Although use of the GEM is not required to apply the Geometric Correction Method, assigning GEM values during grain selection can assist in quickly assessing a sample's overall quality and can help identify potential causes of outlier analyses. The GEM is also an effective teaching tool for those who are new to picking apatite grains, so that the wide spectrum of possible apatite morphologies is clearly communicated.

The corrections and uncertainties in this study were derived from the regression of 2D and 3D measurements of 237 apatite grains displaying a wide variety of morphologies commonly dated for (U-Th)/He thermochronology. The derived corrections and uncertainties were then applied to a set of real data analyzed in the CU TRaIL to determine their impact. The primary outcomes are:

1. There is both uncertainty and systematic error associated with the microscopy approach to calculating V, F_T, and R_{FT} for apatite.
2. The true values of V, F_T, and R_{FT} for apatite are all overestimated by 2D microscopy measurements.

https://doi.org/10.5194/egusphere-2022-1005
Preprint. Discussion started: 18 October 2022

3. All corrections for systematic error and all uncertainties are larger for ellipsoid grains than for hexagonal grains. For both, V has the largest magnitude of overestimation and uncertainty, followed by R_{FT}, and then F_T.
4. For real data, the correction factor for eU typically increases the eU by ~20% with associated 1s uncertainties of 15-16% when both analytical and geometric uncertainties are included. This has important implications for how data are treated during interpretations and during thermal history modeling.
5. For real data, the correction factor for the corrected (U-Th)/He date generally increases the date by 4-9% with associated 1s uncertainties of 3-7% if both analytical and geometric uncertainties are included. Propagating the geometric uncertainty into the corrected date may help account for overdispersion in some (U-Th)/He datasets.

The geometric corrections and geometric uncertainties are substantial enough that they should be routinely included when reporting eU and corrected (U-Th)/He dates to enhance rigorous data interpretation. Ongoing work is using this same approach to quantify appropriate corrections and uncertainties for zircon geometric parameters in (U-Th)/He datasets (Baker et al., 2020).

https://doi.org/10.5194/egusphere-2022-1005
Preprint. Discussion started: 18 October 2022

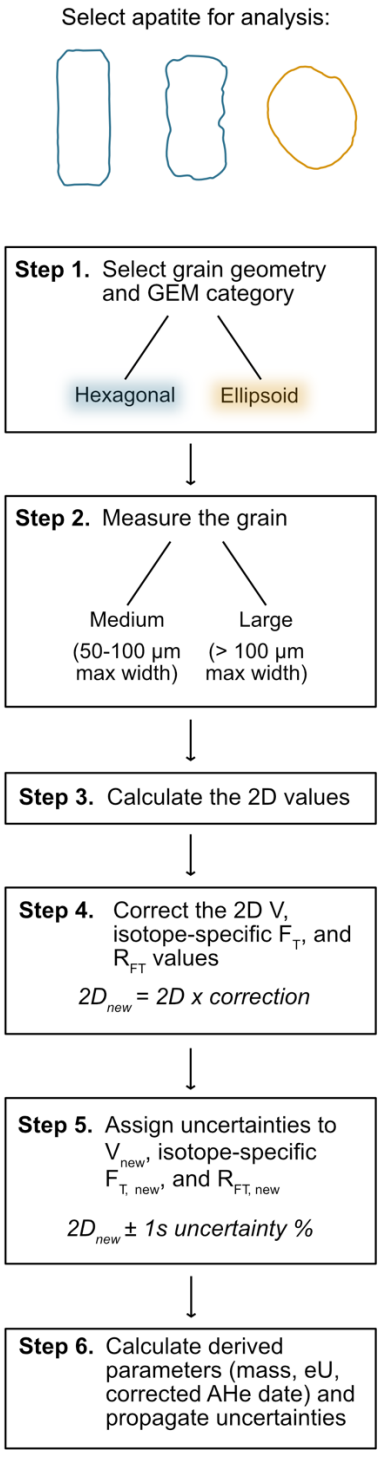

Figure 8. Flow chart outlining workflow for the Geometric Correction Method.

https://doi.org/10.5194/egusphere-2022-1005
Preprint. Discussion started: 18 October 2022

Appendix A: Equations required to use the Geometric Correction Method

All equations necessary to use the corrections and uncertainties are listed below.

Equations for an ellipsoid grain (GEM = C), from Ketcham et al. (2011):

$$V = \frac{4}{3}\pi abc \quad \text{(A1)}$$

$$S = 4\pi\left(\frac{a^p b^p + b^p c^p + c^p a^p}{3}\right)^{1/p} \text{ with p = 1.6075} \quad \text{(A2)}$$

$$F_T = 1 - \frac{3}{4}\frac{S}{R_s} + \left[\frac{1}{16} + 0.1686\left(1 - \frac{a}{R_s}\right)^2\right]\left(\frac{S}{R_s}\right)^3 \quad \text{(A3)}$$

Where S is the stopping distance of an alpha particle for a given parent isotope (18.81, 21.80, and 22.25 µm for ^{238}U, ^{235}U, ^{232}Th, respectively). This equation is used to calculate each isotope-specific F_T value, each with a difference stopping distances.

Equations for a hexagonal (GEM = A or B) grain from Ketcham et al. (2011), modified to reflect the use of only a maximum width (W) and where we use L to denote grain length instead of H. Because only a maximum width is used in the Geometric Correction Method, ΔV is always equal to Equation (4).

$$\Delta V = \frac{1}{6\sqrt{3}}\left(W - \frac{\sqrt{3}}{2}W\right)^3 \quad \text{(A4)}$$

$$V = LW\left(W - \frac{W}{2\sqrt{3}}\right) - N_p\left(\frac{\sqrt{3}}{8}W^3 - \Delta V\right) \quad \text{(A5)}$$

$$S = 2L\left(W + \frac{W}{\sqrt{3}}\right) + 2W\left(W - \frac{W}{2\sqrt{3}}\right) - N_p\left(\frac{\sqrt{3}}{4}W^2 + \left(2 - \sqrt{2}\right)W^2 + \frac{\sqrt{2}-1}{2\sqrt{3}}W^2\right) \quad \text{(A6)}$$

$$F_T = 1 - \frac{3}{4}\frac{S}{R_s} + \left[(0.2093 - 0.0465N_P)\left(W + \frac{W}{\sqrt{3}}\right) + \left(0.1062 + \frac{0.2234S}{S + 6(W\sqrt{3} - W)}\right) \times \left(L - N_P\frac{\frac{W\sqrt{3}}{2} + W}{4}\right)\right]\frac{S^2}{V} \quad \text{(A7)}$$

Where S is the stopping distance of an alpha particle for a given parent isotope (18.81, 21.80, and 22.25 µm for ^{238}U, ^{235}U, ^{232}Th, respectively). This equation is used to calculate each isotope-specific F_T value, each with a difference stopping distances.

Age equation, from Ketcham et al. (2011):

https://doi.org/10.5194/egusphere-2022-1005
Preprint. Discussion started: 18 October 2022

$$^4He = 8F_{T,238}\,{}^{238}U(e^{\lambda_{238}t} - 1) + 7F_{T,235}\,{}^{235}U(e^{\lambda_{235}t} - 1)$$

$$+6F_{T,232}\,{}^{232}Th\left(e^{\lambda_{232}t} - 1\right) + F_{T,147}\,{}^{147}Sm\left(e^{\lambda_{238}t} - 1\right) \quad \text{(A8)}$$

Equation for combined F_T and R_{FT} from Cooperdock et al. (2019):

$$\frac{S}{R} = 1.681 - 2.428F_T + 1.153F_T^2 - 0.406F_T^3 \ (B = 1.31) \quad \text{(A9)}$$

$$A_{238} = (1.04 + 0.247[Th/U])^{-1} \quad \text{(A10)}$$

$$A_{232} = (1 + 4.21/[Th/U])^{-1} \quad \text{(A11)}$$

$$\overline{F_T} = A_{238}F_{T,238} + A_{232}F_{T,232} + (1 - A_{238} - A_{232})F_{T,235} \quad \text{(A12)}$$

$$\overline{S} = A_{238}S_{238} + A_{232}S_{232} + (1 - A_{238} - A_{232})S_{235}, \quad \text{(A13)}$$

where S_{238}, S_{232}, S_{235} are the weighted means stopping distances for each decay chain (18.81, 21.80, and 22.25 µm, respectively, for apatite).

$$R_{FT} = \overline{S}/\left(\frac{S}{R}\right) \quad \text{(A14)}$$

Equation for eU from Cooperdock et al. (2019):

$$eU = [U] + 0.238[Th] + 0.0012[Sm] \ (or\ 0.0083[^{147}Sm]) \quad \text{(A15)}$$

Appendix B: Additional sample information

Table B1. Apatite CT scan parameters

https://doi.org/10.5194/egusphere-2022-1005
Preprint. Discussion started: 18 October 2022

Mount	1	2	3	4	5	6	7	8	9
Objective	20X	20X	20X	20X	20X	20X	20X	20X	20X
Pixel Size (µm)	0.64	0.63	0.63	0.63	0.63	0.64	0.63	0.63	0.63
X-Ray Power (W)	3	3	3	3	3	3	3	3	3
X-Ray Voltage (kV)	40	40	40	40	40	40	40	40	40
Number of Projections	3201	3201	3201	3201	3201	3201	3201	3201	3201
Binning	2	2	2	2	2	2	2	2	2
Filter	Air	Air	Air	Air	Air	Air	Air	Air	Air
Height (µm)	1024	993	993	993	993	993	993	993	993
Width (µm)	1024	993	993	993	993	993	993	993	993
Sample X (µm)	-676	82	-150	-399	-321	192	-848	-334	-210
Sample Y (µm)	-12412	-12602	-12987	-8929	-11251	-9977	-9600	-10860	-9664
Sample Z (µm)	87	106	29	267	884	1605	261	295	425
Sample Theta (°)	-180	-180	-180	-180	-180	-180	-180	-180	-180
Detector To Sample Distance (mm)	5.01	5.17	4.95	4.97	4.99	5.42	5.07	5.08	5.02
Source To Sample Distance (mm)	-4.44	-4.51	-4.33	-4.33	-4.34	-4.75	-4.33	-4.32	-4.38
Exposure (s)	2.1	2.5	2.3	2.3	2.0	2.7	2.3	2.5	2.5
Total Scan Time (h)	3.0	3.4	3.2	3.2	2.9	3.6	3.2	3.4	3.4

840

https://doi.org/10.5194/egusphere-2022-1005
Preprint. Discussion started: 18 October 2022

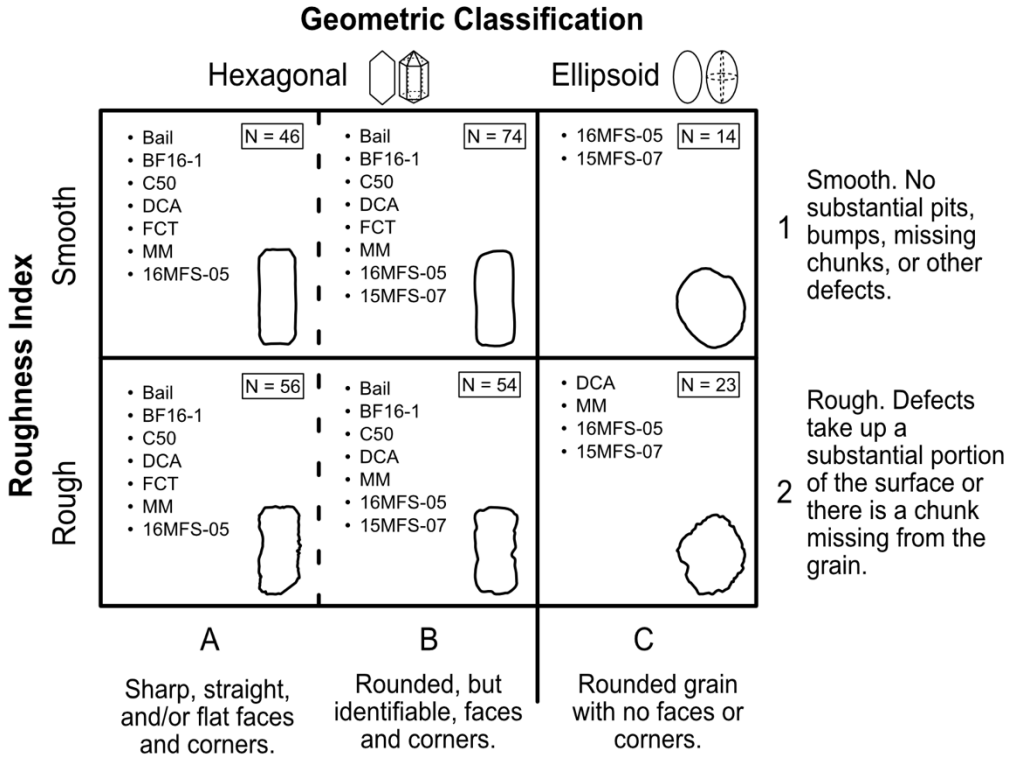

Figure B1. Grain Evaluation Matrix listing the samples and number of grains for which high-quality CT data were acquired in each category.

https://doi.org/10.5194/egusphere-2022-1005
Preprint. Discussion started: 18 October 2022

Appendix C: Additional regression and uncertainty information

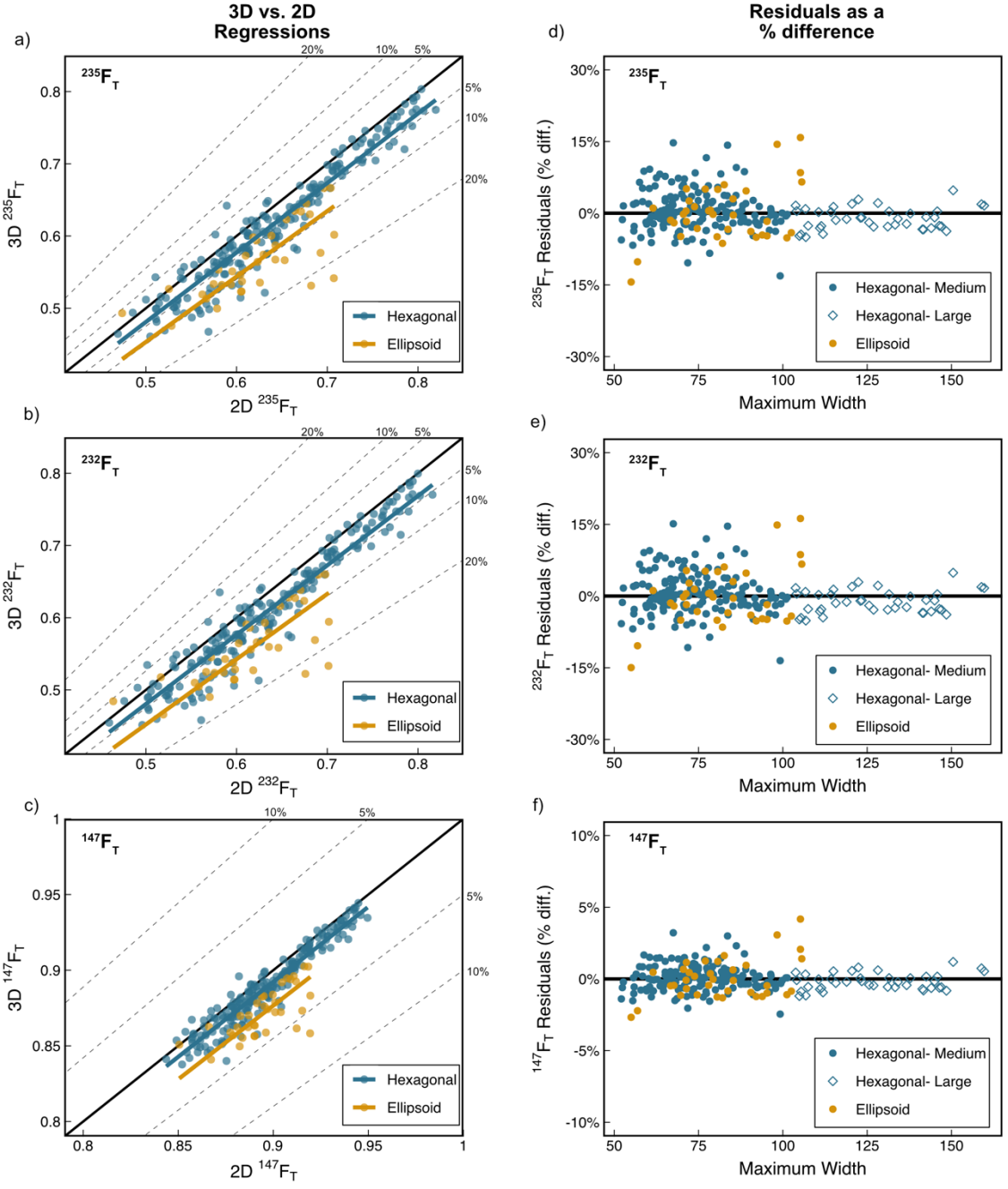

Figure C1. These plots illustrate how the corrections for systematic error and how uncertainties were determined for each parent isotope-specific F_T (except $^{238}F_T$, which is included in Figure 6) Scatter plots of 3D vs. 2D data (N=237) with regression lines and data distinguished by geometry for (a) $^{235}F_T$ (b) $^{232}F_T$, and (c) $^{147}F_T$. Grains with $F_T < 0.5$ were excluded from the regressions. The bold black line is the 1:1 line and the dashed lines mark the percent difference from the 1:1 line. Note that for all regressions, the regression line falls below the 1:1 line, indicating that the 2D-microscopy data overestimate the 3D-CT data. The 2D data can be

https://doi.org/10.5194/egusphere-2022-1005
Preprint. Discussion started: 18 October 2022

corrected for systematic error by multiplying the 2D data by the 3D/2D slope. Plots of the difference of each 2D value from the regression line (i.e., the residual) as a percent difference vs. maximum width with data distinguished by geometry and grain size. The bold black line is 0% difference. The standard deviation of the % difference in the residuals of each group is the uncertainty on the parameter.

Table C1. Results of Tukey's Highly Significant Difference[a] test to determine if different groups of grains have statistically different slopes.

Grouping & Pairs	Difference in Slopes[b]	95% CI[c]	Adjusted P-value[d]
Volume			
GEM: Geometric Classification			
B-A	< 0.001	[-0.001, 0.001]	0.922
C-A	**0.153**	**[0.153, 0.153]**	**< 0.001**
C-B	**0.153**	**[0.153, 0.153]**	**< 0.001**
Size			
Medium-Large	0.011	[-0.007, 0.029]	0.213
GEM: Roughness			
1-2	0.010	[-0.004, 0.024]	0.157
^{238}FT			
GEM: Geometric			
B-A	< 0.001	[-.001, 0.001]	0.922
C-A	**0.153**	**[0.153, 0.153]**	**< 0.001**
C-B	**0.153**	**[0.153, 0.153]**	**< 0.001**
Size			
Medium-Large	0.011	[-0.007, 0.029]	0.231
Roughness			
1-2	0.010	[-.001, 0.001]	0.157
R_{FT}			
GEM: Geometric			
B-A	0	[-.001, 0.001]	1
C-A	**0.055**	**[0.055, 0.055]**	**< 0.001**
C-B	**0.055**	**[0.055, 0.055]**	**< 0.001**
Size			
Medium-Large	0.004	[-.001, 0.001]	0.213
Roughness			
1-2	0.004	[-0.001, 0.009]	0.157

[a] Tukey's Highly Significant Difference tests if slopes are significantly different from each other or not and takes into account the uncertainties on the slopes. Where the null hypothesis, H_0, is $\beta_1 = \beta_2$ and the alternative hypothesis, H_1, is $\beta_1 \neq \beta_2$.

[b] The 95% confidence interval (CI) of the difference in slopes.

[d] A p-value < 0.05 indicates that H_0 can be rejected, i.e., there is a significant difference between the slopes of the pair. If the p-value is > 0.05, this indicates that there is no significant difference between the means of the pair. Bolded pairs of slopes are those with p-values <0.05 and therefore are treated as separate groups.

Table C2. Uncertainty values (1s) for different groupings of physical variables.

https://doi.org/10.5194/egusphere-2022-1005
Preprint. Discussion started: 18 October 2022

Geometry	Size[a]	Roughness	N	Uncertainty
Volume				
Hex.	**Medium & Large**	**1 & 2**	**201**	**20%**
Hex.	Medium	1 & 2	161	20%
Hex.	Medium	1	86	19%
Hex.	Medium	2	75	21%
Hex.	Large	1 & 2	40	23%
Hex.	Large	1	18	15%
Hex.	Large	2	22	28%
Ellip.	**Medium & Large**	**1 & 2**	**36**	**23%**
$^{238}F_T$				
Hex.	Medium & Large	1 & 2	201	3%
Hex.	**Medium**	**1 & 2**	**161**	**3%**
Hex.	Medium	1	86	3%
Hex.	Medium	2	75	4%
Hex.	**Large**	**1 & 2**	**40**	**2%**
Hex.	Large	1	18	1%
Hex.	Large	2	22	2%
Ellip.	**Medium & Large**	**1 & 2**	**36**	**5%**
R_{FT}				
Hex.	**Medium & Large**	**1 & 2**	**201**	**6%**
Hex.	Medium	1 & 2	161	6%
Hex.	Medium	1	86	6%
Hex.	Medium	2	75	6%
Hex.	Large	1 & 2	40	7%
Hex.	Large	1	18	5%
Hex.	Large	2	22	8%
Ellip.	**Medium & Large**	**1 & 2**	**36**	**10%**

[a] Groups in bold are the groups for which uncertainties are reported (i.e., geometry only for V and R_{FT}; geometry and grain size for F_T).

Appendix D:

Table D1. Results of applying geometric corrections and uncertainties (1s) to apatite (U-Th)/He data from samples previously dated in the CU TRaIL.

https://doi.org/10.5194/egusphere-2022-1005
Preprint. Discussion started: 18 October 2022

			Mass				eU						combined F_T						Corrected apatite (U-Th)/He date								R_{FT}			
			$Mass_{orig}$	$Mass_{new}$			eU_{orig}	eU_{new}					$F_{T,orig}$	$F_{T,new}$					$Date_{orig}$			$Date_{new}$					$R_{FT,orig}$	$R_{FT,new}$		
Sample and aliquot [a]	Geo.[b]	Max. Width[c] (µm)	$Mass_{orig}$ [d] (µg)	$Mass_{new}$[e] (µg)	±[f] (µg)	±[g] (%)	eU_{orig}[h] (ppm)	eU_{new}[i] (ppm)	±TAU[j] (ppm)	±TAU[k] (%)	±TAU + geom[l] (ppm)	±TAU + geom[m] (%)	$F_{T,orig}$[n]	$F_{T,new}$[o]	±TAU[p]	±TAU[q] (%)	±TAU + geom[r]	±TAU + geom[s] (%)	$Date_{orig}$[t] (Ma)	±TAU[u] (Ma)	±TAU[v] (%)	$Date_{new}$[w] (Ma)	±TAU[x] (Ma)	±TAU[y] (%)	±TAU + geom[z] (Ma)	±TAU + geom[aa] (%)	$R_{FT,orig}$[ab] (µm)	$R_{FT,new}$[ac] (µm)	±[ad] (µm)	±[ae] (%)
BF16-1																														
a01	Hex.	202	12.1	10.1	2.0	20%	19.1	23.0	0.4	2%	3.3	15%	0.82	0.79	0.00	1%	0.01	1%	41.5	0.4	1%	42.9	0.5	1%	1.0	2%	85	79	5	6%
a02	Hex.	186	10.1	8.4	1.7	20%	15.6	18.8	0.4	2%	2.7	15%	0.81	0.78	0.00	1%	0.01	1%	46.6	0.6	1%	48.2	0.6	1%	1.1	2%	79	74	4	6%
a03	Hex.	188	9.9	8.3	1.7	20%	19.3	23.3	0.4	2%	3.4	15%	0.82	0.79	0.00	1%	0.01	2%	41.4	0.5	1%	42.8	0.6	1%	1.0	2%	81	75	5	6%
a04	Hex.	150	6.5	5.4	1.1	20%	19.7	23.7	0.5	2%	3.4	14%	0.76	0.73	0.00	1%	0.01	2%	46.3	0.7	1%	48.0	0.7	1%	1.2	2%	63	58	3	6%
a05	Hex.	122	3.2	2.7	0.5	20%	21.1	25.4	0.6	2%	3.7	14%	0.73	0.70	0.00	1%	0.01	2%	50.9	0.7	1%	52.7	0.7	1%	1.2	2%	54	51	3	6%
a06	Hex.	189	3.2	2.7	0.5	20%	24.1	29.0	0.5	2%	4.2	14%	0.71	0.69	0.00	1%	0.01	1%	49.1	0.6	1%	50.8	0.6	1%	1.2	2%	52	48	3	6%
a07	Hex.	110	2.6	2.2	0.4	20%	23.4	28.2	0.8	3%	4.1	14%	0.70	0.68	0.01	1%	0.01	2%	52.5	1.0	2%	54.4	1.0	2%	1.5	3%	51	47	3	6%
a08	Hex.	124	2.5	2.1	0.4	20%	32.8	39.5	1.0	3%	5.7	14%	0.69	0.67	0.01	1%	0.01	2%	52.0	1.1	2%	53.9	1.1	2%	1.5	3%	49	45	3	6%
a09	Hex.	106	2.2	1.8	0.4	20%	17.9	21.5	0.7	3%	3.1	15%	0.67	0.65	0.01	1%	0.01	2%	51.3	1.2	2%	53.2	1.3	2%	1.7	3%	46	42	3	6%
a10	Hex.	96	1.7	1.4	0.3	20%	44.4	53.5	1.3	3%	7.9	15%	0.64	0.62	0.01	1%	0.02	3%	50.3	0.8	2%	52.1	0.9	2%	2.0	4%	43	40	2	6%
MM1																														
a01	Hex.	96	5.3	4.4	0.9	20%	15.7	18.9	0.4	2%	2.8	15%	0.74	0.72	0.01	1%	0.02	2%	68.7	1.2	2%	71.1	1.3	2%	2.7	4%	58	54	3	6%
a02	Hex.	168	16.0	13.3	2.7	20%	24.5	29.5	0.4	1%	4.3	14%	0.84	0.81	0.00	0%	0.01	1%	83.0	0.8	1%	85.9	0.8	1%	1.9	2%	91	85	5	6%
a03	Hex.	145	6.9	5.7	1.1	20%	41.5	50.0	0.9	2%	7.2	14%	0.75	0.72	0.00	1%	0.01	2%	119.0	1.4	1%	123.2	1.5	1%	2.8	2%	59	55	3	6%
a04	Hex.	225	20.3	16.8	3.4	20%	42.1	50.7	0.7	1%	7.4	15%	0.86	0.83	0.00	1%	0.01	1%	140.3	1.7	1%	145.2	1.8	1%	3.3	2%	105	98	6	6%
a05	Hex.	107	2.8	2.3	0.5	20%	43.7	52.6	3.4	6%	8.2	16%	0.71	0.68	0.02	3%	0.02	3%	154.2	9.6	6%	159.6	10.0	6%	10.5	7%	51	47	3	6%
a06	Hex.	154	7.2	5.9	1.2	20%	22.7	27.3	1.2	5%	4.2	15%	0.80	0.77	0.01	2%	0.02	2%	87.6	3.9	4%	90.7	4.0	4%	4.4	5%	75	70	4	6%
a07	Hex.	153	7.2	6.0	1.2	20%	34.8	42.0	1.6	4%	6.1	15%	0.80	0.77	0.01	1%	0.02	2%	100.4	3.3	3%	104.0	3.4	3%	4.0	4%	74	68	4	6%
a08	Hex.	154	8.6	7.2	1.4	20%	33.5	40.4	1.4	4%	5.9	15%	0.81	0.78	0.01	1%	0.01	2%	112.2	3.3	3%	116.2	3.4	3%	4.1	4%	77	72	4	6%
a09	Hex.	133	5.3	4.4	0.9	20%	28.5	34.4	1.7	5%	5.2	15%	0.77	0.74	0.01	2%	0.02	2%	111.7	5.4	5%	115.7	5.7	5%	6.1	5%	64	60	4	6%
a10	Hex.	159	10.8	9.0	1.8	20%	19.5	23.5	0.9	4%	3.5	15%	0.82	0.79	0.01	1%	0.02	2%	92.1	3.4	4%	95.4	3.5	4%	4.0	4%	82	76	5	6%
16MFS05																														
a02	Ellip.	74	1.5	1.1	0.3	23%	48.9	66.1	1.0	2%	10.8	16%	0.66	0.60	0.00	1%	0.02	4%	3.0	0.1	3%	3.3	0.1	3%	0.2	6%	43	37	4	10%
a03	Ellip.	79	1.2	0.9	0.2	23%	80.0	108.1	3.2	3%	17.8	16%	0.65	0.60	0.01	1%	0.02	4%	3.0	0.1	3%	3.2	0.08	2%	0.2	6%	43	36	4	10%
a04	Ellip.	79	1.2	0.9	0.2	23%	15.3	20.7	0.7	3%	3.4	17%	0.65	0.60	0.01	1%	0.02	4%	4.8	0.3	6%	5.3	0.33	6%	0.4	8%	42	36	4	10%
a05	Ellip.	91	1.3	1.0	0.2	23%	42.0	56.7	1.3	2%	9.2	16%	0.66	0.61	0.00	1%	0.02	4%	4.8	0.1	3%	5.2	0.14	3%	0.3	6%	45	38	4	10%

https://doi.org/10.5194/egusphere-2022-1005
Preprint. Discussion started: 18 October 2022

All uncertainties reported at the 1s level.

All calculations done assuming F_T uncertainties are fully correlated (r = 1).

[a] All BF16-1, MM1, and 16MFS05 data are published in Flowers and Kelley (2011), Weisberg et al. (2018), and Collett et al. (2019), respectively.

[b] Geometry is defined as described in Figure 3 of Ketcham et al. (2011). All GEM A and B grains are hexagonal (hex.) and all GEM C grains are ellipsoid (ellip.).

[c] Maximum width is measured perpendicular to the c-ais.

[d] $Mass_{orig}$ is the mass of the crystal determined by 2D microscopy measurements, the volume assuming the reported grain geometry, and the volume equations and mineral densities in Ketcham et al. (2011)

[e] $Mass_{new}$ is computed the same as $mass_{orig}$, but the original V is corrected by applying the correction factor in Table 2 based on the grain geometry, and this new volume is used in the mass calculation.

[f] The 1s uncertainty on $mass_{new}$ is calculated by propagating the uncertainty on V from Table 2 based on grain geometry through the mass equation.

[g] The 1s percent uncertainty on $mass_{new}$.

[h] eU_{orig} is effective Uranium concentration calculated using the $mass_{orig}$. Calculated as U + 0.238*Th + 0.0012*Sm after equation A7 of Cooperdock et al. (2019).

[i] eU_{new} is computed the same as eU_{orig} but uses the $mass_{new}$ value.

[j] The 1s total analytical uncertainty (TAU, which are the uncertainties on the parent isotopes) on eU. This calculation ignores the negligible contribution from Sm concentration uncertainty and uses 0% geometric uncertainty.

[k] The 1s total analytical percent uncertainty on eU_{new}.

[l] The 1s TAU + geometric uncertainty on eU_{new}. This calculation uses the uncertainty assigned based on grain geometry (Table 2), assumes that the geometric uncertainties on U and Th concentrations are perfectly correlated, and ignores the negligible contribution from Sm concentration uncertainty. Although the correlation coefficient will vary with each data set, the dominant contribution to concentration uncertainty comes from the volumetric uncertainty, which is highly correlated. Additionally, assuming perfect correlation yields the maximum possible value, so we use this conservative approach.

[m] The 1s total analytical + geometric percent uncertainty on eU_{new}.

[n] $F_{T,orig}$ is the combined alpha-ejection correction for the crystal calculated from the original parent isotope-specific F_T corrections, the proportion of U and Th contributing to the ^4He production, and assuming homogeneous parent isotope distributions using equation A4 in Cooperdock et al. (2019). The parent isotope-specific alpha ejection-corrections were computed assuming the reported grain geometry in this table and the equations and alpha-stopping distances in Ketcham et al. (2011).

[o] $F_{T,new}$ is computed the same as $F_{T,orig}$ but uses isotope-specific $F_{T,new}$ values corrected by applying the correction factors in Table 2 based on grain geometry and size.

[p] The 1s TAU on $F_{T,new}$. This calculation uses 0% geometric uncertainty.

[q] The 1s total analytical percent uncertainty on $F_{T,new}$.

[r] The 1s TAU + geometric uncertainty. This calculation uses the parent isotope-specific $F_{T,new}$ uncertainties assigned based on grain geometry and size (Table 2).

[s] The 1s total analytical + geometric percent uncertainty on $F_{T,new}$.

https://doi.org/10.5194/egusphere-2022-1005
Preprint. Discussion started: 18 October 2022

[t] **The corrected (U-Th)/He $date_{orig}$ is calculated iteratively using the absolute values of He, U, Th, Sm, the isotope-specific $F_{T,orig}$ values, and equation 34 in Ketcham et al. (2011) assuming secular equilibrium.**

[u] **The 1s TAU uncertainty on $date_{orig}$ includes the propagated total analytical uncertainties on the U, Th, Sm and He measurements. Uncertainty propagation done using HeCalc (Martin et al., in review).**

[v] **The 1s total analytical percent uncertainty on $date_{orig}$.**

[w] **The corrected (U-Th)/He $date_{new}$ is computed the same as $date_{orig}$, but uses the isotope-specific $F_{T,new}$ values corrected by applying the correction factors in Table 2 based on grain geometry and size.**

[x] **The 1s TAU uncertainty on the corrected (U-Th)/He $date_{new}$ includes the propagated total analytical uncertainties on the U, Th, Sm, He measurements (Table 2). This calculation uses 0% geometric uncertainty. Uncertainty propagation done using HeCalc (Martin et al., in review).**

[y] **The 1s total analytical percent uncertainty on the corrected (U-Th)/He $date_{new}$.**

[z] **The 1s total analytical + geometric uncertainty on the corrected (U-Th)/He $date_{new}$. This calculation uses the parent isotope-specific $F_{T,new}$ uncertainties assigned based on grain geometry and size (Table 2).**

[aa] **The 1s total analytical + geometric percent uncertainty on the corrected (U-Th)/He $date_{new}$.**

[ab] **$R_{FT,orig}$ is the radius of a sphere with an equivalent alpha-ejection correction as the grain, calculated using the uncorrected parent isotope-specific FT values in equation A6 in Cooperdock et al. (2019).**

[ac] **$R_{FT,new}$ is computed from $R_{FT,orig}$ by multiplying $R_{FT,orig}$ by the correction factor in Table 2 based on grain geometry.**

[ad] **The 1s uncertainty on $R_{FT,new}$ is assigned based on grain geometry (Table 2).**

[ae] **The 1s percent uncertainty on $R_{FT,orig}$.**

Code and Data Availability

Data and code used to produce the corrections and uncertainties and figures is stored through the Open Science Framework: https://osf.io/fu98s/. All analyses and plots were done in R (Wickham et al., 2019).

Author Contributions

RMF and JRM conceptualized the project; SDZ curated the data; SDZ and JRM performed the formal data analysis; RMF, JRM, and SDZ acquired funding; SDZ performed the investigation; JRM, SDZ, and RMF developed the methodology; RMF provided supervision; SDZ performed the validation; SDZ did the data visualizations; SDZ and RMF wrote the original draft; RMF, SDZ, and JRM reviewed and edited the manuscript.

Competing Interests

The authors declare they have no conflict of interest.

https://doi.org/10.5194/egusphere-2022-1005
Preprint. Discussion started: 18 October 2022

Acknowledgments

We thank Alison Duvall, Lon Abbott, Ray Donelick, and Jacky Baughman for samples. We are grateful to Jennifer Coulombe and Adrian Gestos for their assistance, support, and advice regarding nano-CT and Dragonfly. The use of Blob3D would not have been possible without support from Rich Ketcham and Romy D. Hanna. We appreciate numerous discussions with Morgan Baker. Finally, thanks to Peter Martin for advice and for HeCalc. This work was partially funded by National Science Foundation GRFP DGE-1650115 to Zeigler. Funding for the Zeiss Xradia Versa X-Ray Microscope was provided by NSF CMMI-1726864.

References

Abbey, A. L., Niemi, N. A., Geissman, J. W., Winkelstern, I. Z., and Heizler, M.: Early Cenozoic exhumation and paleotopography in the Arkansas River valley, southern Rocky Mountains, Colorado, Lithosphere, 10, 239–266, https://doi.org/10.1130/L673.1, 2017.

Abbott, L. D., Flowers, R. M., Metcalf, J., Falkowski, S., and Niazy, F.: Post-Laramide, Eocene epeirogeny in central Colorado—The result of a mantle drip?, Geosphere, 18, 1223–1246, https://doi.org/10.1130/GES02434.1, 2022.

Baker, M., Zeigler, S. D., Metcalf, J. R., and Flowers, R. M.: Estimating Uncertainties for Alpha-Ejection Corrections and eu Values for the Zircon U-Th Method, in: Fall Meeting 2020, American Geophysical Union, Online, https://doi.org/2020AGUFMV031.0004B, 2020.

Baughman, J. S., Flowers, R. M., Metcalf, J. R., and Dhansay, T.: Influence of radiation damage on titanite He diffusion kinetics, Geochimica et Cosmochimica Acta, 205, 50–64, https://doi.org/10.1016/j.gca.2017.01.049, 2017.

Brown, R. W., Beucher, R., Roper, S., Persano, C., Stuart, F., and Fitzgerald, P.: Natural age dispersion arising from the analysis of broken crystals. Part I: Theoretical basis and implications for the apatite (U–Th)/He thermochronometer, Geochimica et Cosmochimica Acta, 122, 478–497, https://doi.org/10.1016/j.gca.2013.05.041, 2013.

Collett, C. M., Duvall, A. R., Flowers, R. M., Tucker, G. E., and Upton, P.: The Timing and Style of Oblique Deformation Within New Zealand's Kaikōura Ranges and Marlborough Fault System Based on Low-Temperature Thermochronology, Tectonics, 38, 1250–1272, https://doi.org/10.1029/2018TC005268, 2019.

Cooperdock, E. H. G., Ketcham, R. A., and Daniel F. Stockli: Resolving the effects of 2-D versus 3-D grain measurements on apatite (U–Th)/He age data and reproducibility, Geochronology, 1, 17–41, https://doi.org/10.5194/gchron-1-17-2019, 2019.

https://doi.org/10.5194/egusphere-2022-1005
Preprint. Discussion started: 18 October 2022

Dragonfly. Object Research Systems. Montréal, Quebec, Canada. https://theobjects.com/dragonfly, 2020.

Ehlers, T. A. and Farley, K. A.: Apatite (U–Th)/He thermochronometry: methods and applications to problems in tectonic and surface processes, Earth and Planetary Science Letters, 206, 1–14, https://doi.org/10.1016/S0012-821X(02)01069-5, 2003.

Evans, N. J., McInnes, B. I. A., Squelch, A. P., Austin, P. J., McDonald, B. J., and Wu, Q.: Application of X-ray micro-computed tomography in (U–Th)/He thermochronology, Chemical Geology, 257, 101–113, https://doi.org/10.1016/j.chemgeo.2008.08.021, 2008.

Farley, K. A., Wolf, R. A., and Silver, L. T.: The effects of long alpha-stopping distances on (U-Th)/He ages, Geochimica et Cosmochimica Acta, 60, 4223–4229, https://doi.org/10.1016/S0016-7037(96)00193-7, 1996.

Flowers, R. M. and Kelley, S. A.: Interpreting data dispersion and "inverted" dates in apatite (U–Th)/He and fission-track datasets: An example from the US midcontinent, Geochimica et Cosmochimica Acta, 75, 5169–5186, https://doi.org/10.1016/j.gca.2011.06.016, 2011.

Flowers, R. M., Shuster, D. L., Wernicke, B. P., and Farley, K. A.: Radiation damage control on apatite (U-Th)/He dates from the Grand Canyon region, Colorado Plateau, Geology, 35, 447–450, https://doi.org/10.1130/G23471A.1, 2007.

Flowers, R. M., Zeitler, P. K., Danišík, M., Reiners, P. W., Gautheron, C., Ketcham, R. A., Metcalf, J. R., Stockli, D. F., Enkelmann, E., and Brown, R. W.: (U-Th)/He chronology: Part 1. Data, uncertainty, and reporting, Geological Society of America Bulletin, 130, 33, 2022a.

Flowers, R. M., Ketcham, R. A., Enkelmann, E., Gautheron, C., Reiners, P. W., Metcalf, J. R., Danišík, M., Stockli, D. F., and Brown, R. W.: (U-Th)/He chronology: Part 2. Considerations for evaluating, integrating, and interpreting conventional individual aliquot data, Geological Society of America Bulletin, 130, 25, 2022b.

Gleadow, A., Harrison, M., Kohn, B., Lugo-Zazueta, R., and Phillips, D.: The Fish Canyon Tuff: A new look at an old low-temperature thermochronology standard, Earth and Planetary Science Letters, 424, 95–108, https://doi.org/10.1016/j.epsl.2015.05.003, 2015.

Glotzbach, C., Lang, K. A., Avdievitch, N. N., and Ehlers, T. A.: Increasing the accuracy of (U-Th(-Sm))/He dating with 3D grain modelling, Chemical Geology, 506, 113–125, https://doi.org/10.1016/j.chemgeo.2018.12.032, 2019.

Harbert, S. A.: Landscape Response to Oblique Convergence: Insights from Numerical Modeling and from the Marlborough Fault System, New Zealand, Thesis, https://digital.lib.washington.edu:443/researchworks/handle/1773/44635, 2019.

https://doi.org/10.5194/egusphere-2022-1005
Preprint. Discussion started: 18 October 2022

Herman, F., Braun, J., Senden, T. J., and Dunlap, W. J.: (U–Th)/He thermochronometry: Mapping 3D geometry using micro-X-ray tomography and solving the associated production–diffusion equation, Chemical Geology, 242, 126–136, https://doi.org/10.1016/j.chemgeo.2007.03.009, 2007.

Hoffman, P. F.: United Plates of America, The Birth of a Craton: Early Proterozoic Assembly and Growth of Laurentia, Annual Review of Earth and Planetary Sciences, 16, 543–603, https://doi.org/10.1146/annurev.ea.16.050188.002551, 1988.

Hourigan, J. K., Reiners, P. W., and Brandon, M. T.: U-Th zonation-dependent alpha-ejection in (U-Th)/He chronometry, Geochimica et Cosmochimica Acta, 69, 3349–3365, https://doi.org/10.1016/j.gca.2005.01.024, 2005.

JCGM: Joint Committee for Guides in Metrology – The International Vocabulary of Metrology – Basic and General Concepts and Associated Terms, 2012.

Ketcham, R. A.: Computational methods for quantitative analysis of three-dimensional features in geological specimens, Geosphere, 1, 32–41, https://doi.org/10.1130/GES00001.1, 2005.

Ketcham, R. A. and Ryan, T. M.: Quantification and visualization of anisotropy in trabecular bone, Journal of Microscopy, 213, 158–171, https://doi.org/10.1111/j.1365-2818.2004.01277.x, 2004.

Ketcham, R. A., Gautheron, C., and Tassan-Got, L.: Accounting for long alpha-particle stopping distances in (U–Th–Sm)/He geochronology: Refinement of the baseline case, Geochimica et Cosmochimica Acta, 75, 7779–7791, https://doi.org/10.1016/j.gca.2011.10.011, 2011.

Martin, P. E., Metcalf, J. R., and Flowers, R. M.: Calculation of Uncertainty in the (U-Th)/He System, Geochronological data analysis/statistics/modelling, https://doi.org/10.5194/egusphere-2022-299, in review.

Meesters, A. G. C. A. and Dunai, T. J.: Solving the production–diffusion equation for finite diffusion domains of various shapes: Part II. Application to cases with α-ejection and nonhomogeneous distribution of the source, Chemical Geology, 186, 57–73, https://doi.org/10.1016/S0009-2541(01)00423-5, 2002.

Rattenbury, M. S., Townsend, D. B., and Johnston, M. R.: Geology of the Kaikoura area, Institute of Geological & Nuclear Sciences (NZ), 2006.

Rodgers, D. W.: Thermal and Structural Evolution of the Southern Deep Creek Range, West Central Utah and East Central Nevada., 1, 1988.

https://doi.org/10.5194/egusphere-2022-1005
Preprint. Discussion started: 18 October 2022

Shuster, D. L., Flowers, R. M., and Farley, K. A.: The influence of natural radiation damage on helium diffusion kinetics in apatite, Earth and Planetary Science Letters, 249, 148–161, https://doi.org/10.1016/j.epsl.2006.07.028, 2006.

Spell, T. L. and McDougall, I.: Characterization and calibration of 40Ar/39Ar dating standards, Chemical Geology, 198, 189–211, https://doi.org/10.1016/S0009-2541(03)00005-6, 2003.

Van Schmus, W. R., Bickford, M. E., and Zietz, I.: Early and Middle Proterozoic provinces in the central United States, in: Geodynamics Series, vol. 17, edited by: Kröner, A., American Geophysical Union, Washington, D. C., 43–68, https://doi.org/10.1029/GD017p0043, 1987.

Weisberg, W. R., Metcalf, J. R., and Flowers, R. M.: Distinguishing slow cooling versus multiphase cooling and heating in zircon and apatite (U-Th)/He datasets: The case of the McClure Mountain syenite standard, Chemical Geology, 485, 90–99, https://doi.org/10.1016/j.chemgeo.2018.03.038, 2018.

Wickham, H., Averick, M., Bryan, J., Chang, W., McGowan, L. D., François, R., Grolemund, G., Hayes, A., Henry, L., Hester, J., Kuhn, M., Pedersen, T. L., Miller, E., Bache, S. M., Müller, K., Ooms, J., Robinson, D., Seidel, D. P., Spinu, V., Takahashi, K., Vaughan, D., Wilke, C., Woo, K., and Yutani, H.: Welcome to the tidyverse, Journal of Open Source Software, 4, 1686, https://doi.org/10.21105/joss.01686, 2019.